

1 Importance of Aerosol Composition and Aerosol Vertical Profile in Global 2 Spatial Variation of the PM_{2.5} to AOD Relationship

3 Haihui Zhu^{1*}, Randall V. Martin¹, Aaron van Donkelaar¹, Melanie S. Hammer¹, Chi Li¹, Jun Meng²,
4 Christopher R. Oxford¹, Xuan Liu¹, Yanshun Li¹, Dandan Zhang¹, Inderjeet Singh¹, Alexei Lyapustin³

5 ¹Department of Energy, Environmental & Chemical Engineering, Washington University in St. Louis, St.
6 Louis, MO, USA

7 ²Department of Civil and Environmental Engineering, Washington State University, Pullman, WA, USA

8 ³Laboratory for Atmospheres, NASA Goddard Space Flight Center, Greenbelt, MD, USA

9 *Correspondence:* Haihui Zhu (haihuizhu@wustl.edu)

10 **Abstract** Ambient fine particulate matter (PM_{2.5}) is the leading global environmental determinant
11 of mortality. However, large gaps exist in ground-based PM_{2.5} monitoring. Satellite remote sensing
12 of aerosol optical depth (AOD) offers information to fill these gaps worldwide, when augmented
13 with a modeled PM_{2.5} to AOD relationship. This study aims to understand the spatial pattern and
14 driving factors of the relationship by examining η ($= \frac{PM_{2.5}}{AOD}$), from both observations and modeling.
15 A global observational estimate of η for the year 2019 is inferred from 6,870 ground-based PM_{2.5}
16 measurement sites and satellite retrieved AOD. The GEOS-Chem global chemical transport model
17 in its high performance configuration (GCHP), is used to interpret the observed spatial pattern of
18 annual mean η . Measurements and the GCHP simulation consistently identify a global population-
19 weighted mean η of 96-98 $\mu\text{g}/\text{m}^3$, with regional values ranging from 59.8 $\mu\text{g}/\text{m}^3$ in North America
20 to more than 190 $\mu\text{g}/\text{m}^3$ in Africa. The highest η is found in arid regions where aerosols are less
21 hygroscopic due to mineral dust, followed by regions strongly influenced by surface aerosol
22 sources. Relatively low η is found over regions distant from strong aerosol sources. The spatial
23 correlation of observed η with meteorological fields, aerosol vertical profiles, and aerosol chemical
24 composition reveals that the spatial variation of η is strongly influenced by aerosol composition
25 and aerosol vertical profile. Sensitivity tests with globally uniform parameters quantify their
26 effects on η spatial variability, with a population-weighted mean difference of 12.3 $\mu\text{g}/\text{m}^3$ for
27 aerosol composition that reflects the determinant composition effects on aerosol hygroscopicity
28 and aerosol optical properties; and a population-weighted mean difference of 8.4 $\mu\text{g}/\text{m}^3$ for aerosol
29 vertical profile that reflects spatial variation in the column to surface relationship.

30 **1 Introduction**

31 Exposure to ambient fine particulate matter (PM_{2.5}) has been recognized as the predominant
32 environmental risk factor for the global burden of disease, leading to millions of deaths annually
33 (Brauer et al., 2024). Even at low PM_{2.5} concentrations, long-term exposure can increase
34 circulatory and respiratory related mortality (Christidis et al., 2019; Pinault et al., 2016;
35 Weichenthal et al., 2022). Despite the importance of PM_{2.5}, many of the world’s countries do not
36 provide publicly accessible PM_{2.5} data (Martin et al., 2019). Satellite remote sensing of aerosol
37 optical depth (AOD), an optical measure of aerosol abundance, offers information about the
38 distribution of PM_{2.5} (Kondragunta et al., 2022). A large community relies upon the spatial
39 distribution of PM_{2.5} concentrations inferred from satellite AOD and a modeled PM_{2.5} to AOD
40 relationship, for health impact assessment and epidemiological analyses of long-term exposure
41 (Brauer et al., 2024; Burnett et al., 2018; Cohen et al., 2017; Hao et al., 2023). Quantitative
42 application of satellite AOD for long-term characterization of the spatial distribution of PM_{2.5}
43 would benefit from a better understanding of the factors affecting the PM_{2.5}-AOD relationship.

44 The relationship between satellite AOD and surface PM_{2.5} can be established through a statistical
45 method, a geophysical method, or their combination. A statistical method uses ground-based
46 monitors for training and is well suited for regions with dense monitors (Di et al., 2016; Hu et al.,
47 2014; Xin et al., 2014). A geophysical approach utilizes a chemical transport model to simulate
48 the relationship (η) between PM_{2.5} and AOD for application to satellite AOD (van Donkelaar et
49 al., 2006, 2010; He et al., 2021), and thus depends on accurate model representation of η . Van
50 Donkelaar et al. (2015, 2016) combined the two methods by applying geographically weighted
51 regression (GWR) on the geophysical PM_{2.5}, which further constrains geophysical PM_{2.5} using
52 ground measurements and other predictors. However, accuracy of geophysical PM_{2.5} remains
53 critical over vast areas with sparse monitoring, and knowledge about the factors affecting η spatial
54 variability are needed to guide improvements of modeled η and geophysical PM_{2.5}.

55 Previous studies have identified several factors that affect η variability, including aerosol vertical
56 distribution, aerosol hygroscopicity, aerosol optical properties, and ambient meteorological factors
57 such as relative humidity (RH), planetary boundary layer height (PBLH), wind speed, temperature,
58 and fire events (van Donkelaar et al., 2013; Ford and Heald, 2015; Guo et al., 2017; Jin et al., 2019;
59 Li et al., 2015; Wendt et al., 2023). Most studies focused on the temporal variability of η and found

60 association with meteorological variables such as PBLH (Chu et al., 2015; Damascena et al., 2021;
61 Gupta et al., 2006; He et al., 2021; Yang et al., 2019; Zhang et al., 2009). A few studies have
62 examined the regional-scale spatial variation of η with meteorological, land type variables, and
63 aerosol vertical profile in North America (van Donkelaar et al., 2006; Jin et al., 2020; Li et al.,
64 2015) and China (Yang et al., 2019). To our knowledge, none have examined the factors at the
65 global scale affecting the spatial variation of η or the effects of chemical composition.

66 In this work, we examine this knowledge gap about the spatial variation in η at a global scale. We
67 first collect data from more than 6,000 $PM_{2.5}$ monitoring sites provided by ten networks and
68 satellite AOD to obtain an observationally based map of η . We further interpret the global η
69 distribution using the GEOS-Chem model of atmospheric composition with recent improvements
70 in aerosol size representation, $PM_{2.5}$ diel variation, and vertical allocation. By decomposing the
71 simulated η , we identify 2 strong drivers of η spatial variability: aerosol composition and aerosol
72 vertical profile. We conduct sensitivity tests using GEOS-Chem to study how the two factors vary
73 globally and how they contribute to the spatial variation in η .

74 **2 Methods**

75 **2.1 Ground Measured $PM_{2.5}$**

76 We collect ground-based measurements of $PM_{2.5}$ for the year 2019 to produce observational
77 constraints on η ($\frac{PM_{2.5}}{AOD}$), the spatially and temporally varying ratio between 24-hour surface $PM_{2.5}$
78 concentrations and total column AOD at satellite sampling time. At the time of manuscript
79 preparation, the year 2019 offered the greatest density of measurements and the most current
80 emission inventory. We obtain $PM_{2.5}$ measurements from 7 regional networks and 3 global
81 networks, as shown in Figure A1. For the United States, we access data from the United States
82 Environmental Protection Agency's Air Quality System ([https://www.epa.gov/outdoor-air-](https://www.epa.gov/outdoor-air-quality-data/download-daily-data)
83 [quality-data/download-daily-data](https://www.epa.gov/outdoor-air-quality-data/download-daily-data)), including both Federal Reference Method and non-Federal
84 Reference Methods $PM_{2.5}$ (e.g. IMPROVE network). $PM_{2.5}$ data for Canada are from the
85 Environment Canada's National Air Pollution Surveillance (NAPS) program. $PM_{2.5}$ data for
86 Europe are from the European Environment Agency Air Quality e-Reporting system
87 (<https://www.eea.europa.eu/data-and-maps/data/aqreporting>). Over mainland China, $PM_{2.5}$

88 measurements from the National and Provincial Environmental Protection Agencies are
89 downloaded from <http://beijingair.sinaapp.com/>. Over India, PM_{2.5} data are originally from the
90 Central Pollution Control Board Continuous Ambient Air Quality Monitoring network and the U.S.
91 embassies. Over Australia, observations are downloaded for the Northern Territory
92 (<http://ntepa.webhop.net/NTEPA/>), Queensland (<https://www.data.qld.gov.au/dataset/>), and New
93 South Wales ([https://www.dpie.nsw.gov.au/air-quality/air-quality-data-services/data-download-](https://www.dpie.nsw.gov.au/air-quality/air-quality-data-services/data-download-facility)
94 [facility](https://www.dpie.nsw.gov.au/air-quality/air-quality-data-services/data-download-facility)). We require at least 5 days of measurements for each month for a monitor to be included.
95 Additionally, we obtain PM_{2.5} measurements over other regions provided by the World Health
96 Organization (WHO) Global Ambient Air Quality Database
97 (<https://www.who.int/data/gho/data/themes/air-pollution/who-air-quality-database/2022>),
98 OpenAQ (<https://openaq.org/>), and the Surface PARTiculate mAtter Network (SPARTAN,
99 <https://www.spartan-network.org/>), which is co-located with the Aerosol Robotic Network
100 (AERONET). SPARTAN also provides filter based PM_{2.5} chemical composition, which is initially
101 described in Snider et al., (2016). Subsequent developments to the sampling and analysis
102 procedure of SPARTAN include an upgrade to the AirPhoton SS5 sampling station to use a
103 cyclone inlet, an automated weighing system (MTL AH500E) to improve precision and throughput,
104 additional black carbon analysis by Hybrid Integrating Plate/Sphere (White et al., 2016), elements
105 measured by X-ray Fluorescence (Liu et al., 2024) and a global mineral dust equation (Liu et al.,
106 2022). We require at least 50 days of coincident PM_{2.5} and AERONET AOD measurements for a
107 SPARTAN site to be included in our analysis.

108 We also collected publicly available PM_{2.5} compositional data to assess GCHP simulated
109 composition. Long-term PM_{2.5} compositional data are included from the United States
110 Environmental Protection Agency's Air Quality System, the European Environment Agency Air
111 Quality e-Reporting system, and SPARTAN, with a total of 365 sites covering the U.S. (306),
112 Europe (37), and the Global South (22).

113 **2.2 Satellite AOD**

114 We obtain AOD at 550 nm from the Multi-Angle Implementation of Atmospheric Correction
115 (MAIAC) algorithm, which offers AOD at a high spatial resolution of 1 km worldwide over both
116 land and coastal regions (Lyapustin et al., 2018). The radiances used in the retrieval are measured

117 by the twin MODerate resolution Imaging Spectroradiometer (MODIS) instruments onboard the
118 Terra and Aqua satellites. Terra follows a descending orbital path, crossing the equator at 10:30
119 local time, while Aqua is on an ascending orbit with 13:30 equatorial crossing local time. Both
120 MODIS instruments offer a wide swath width of 2330 km, enabling nearly global daily coverage
121 of the Earth (Sayer et al., 2014). PM_{2.5} monitoring sites with annual mean satellite AOD less than
122 0.05 (background AOD level over land) are excluded to reduce the influence of retrieval
123 uncertainties on our analysis.

124 **2.3 AERONET AOD**

125 AERONET is a worldwide sun photometer network that provides long-term measurement of AOD.
126 We use the Version 3 Level 2 database, which includes an improved cloud screening algorithm
127 (Giles et al., 2019). We sample AERONET AOD within ± 15 min of the satellite overpass time and
128 interpolate to 550 nm wavelength, based on the local Ångström exponent at 440 and 670 nm. For
129 SPARTAN sites, we sample AERONET data coincidentally with SPARTAN aerosol composition
130 to obtain the ground-based observation of η .

131 **2.4 GEOS-Chem Simulation**

132 We simulate η with the GEOS-Chem chemical transport model (www.geos-chem.org, last access:
133 26 October 2023), driven by offline meteorological data, MERRA-2, from the Goddard Earth
134 Observing System (GEOS) of the NASA Global Modeling and Assimilation Office (Schubert et
135 al., 1993). We use the high-performance configuration of GEOS-Chem (GCHP) (Eastham et al.,
136 2018) version 13.4.0 (DOI: 10.5281/zenodo.7254268), which includes advances in performance
137 and usability (Martin et al., 2022). The simulation is conducted for the year 2019, on a C90 cubed-
138 sphere grid corresponding to a horizontal resolution of about 100 km, with a spin-up time of 1
139 month.

140 The GEOS-Chem aerosol simulation includes the sulfate-nitrate-ammonium (SNA) system
141 (Fountoukis and Nenes, 2007), primary and secondary carbonaceous aerosols (Pai et al., 2020;
142 Park et al., 2003; Wang et al., 2014), sea salt (Jaeglé et al., 2011), and natural (Fairlie et al., 2007;
143 Meng et al., 2021) and anthropogenic (Philip et al., 2017) dust. Emissions are processed with the
144 Harmonized Emissions Component (HEMCO) (Lin et al., 2021). The primary emission data are

145 from the Community Emissions Data System version 2 (CEDSV₂; Hoesly et al., 2018; CEDS, 2024)
146 for the year 2019. Emissions from stacks are distributed vertically (Bieser et al., 2011). Diel
147 variation of anthropogenic emissions is included (Li et al., 2023). Resolution-dependent soil NO_x,
148 sea salt, biogenic VOC, and natural dust emissions are calculated offline at native meteorological
149 resolution to produce consistent emissions across resolutions (Meng et al., 2021; Weng et al.,
150 2020). Biomass burning emissions use the Global Fire Emissions Database, version 4 (GFED4) at
151 daily resolution (van der Werf et al., 2017) for the year 2019. We estimate organic matter (OM)
152 from primary organic carbon using an OM/OC parameterization (Canagaratna et al., 2015; Philip
153 et al., 2014b). For secondary aerosol components, the concentration at 2 m above the surface is
154 used to calculate PM_{2.5}, following Li et al. (2023). A 50% reduction of the surface nitrate
155 concentration is applied to account for the long-standing bias in surface nitrate simulated by
156 GEOS-Chem (Heald et al., 2012; Miao et al., 2020; Travis et al., 2022; Zhai et al., 2021; Zhang et
157 al., 2012; also Figure A2 in this manuscript) and other models such as CMAQ (Shimadera et al.,
158 2014), WRF-Chem (Sha et al., 2019), and EMEP/MSC-W (Prank et al., 2016). Despite this bias,
159 GEOS-Chem can sufficiently represent the variability of nitrate for applications to studies at global
160 (McDuffie et al., 2021; Weagle et al., 2018) and regional (Geng et al., 2017; Kim et al., 2015;
161 Philip et al., 2014a; Zhai et al., 2021) scales. Dry and wet deposition follows Amos et al. (2012),
162 with a standard resistance-in-series dry deposition scheme (Wang et al., 1998). Wet deposition
163 includes scavenging processes from convection and large-scale precipitation (Liu et al., 2001).

164 Global RH-dependent aerosol optical properties are based on the Global Aerosol Data Set (GADS)
165 (Kopke et al., 1997), as originally implemented by Martin et al. (2003), with updates for SNA and
166 OM dry size (Zhu et al., 2023), hygroscopicity (Latimer and Martin, 2019), mineral dust size
167 distribution (Zhang et al., 2013), and absorbing brown carbon (Hammer et al., 2016). These
168 updates enable GEOS-Chem to capture 74% of the AOD spatial variability versus AERONET
169 (Zhu et al., 2023). A slight systematic low bias against MAIAC AOD is found, with an intercept
170 of -0.05 and a population-weighted mean difference (PWMD) of -0.04. Low bias in simulated
171 AOD is also reported for other models, such as CMAQ (Jin et al., 2019) and WRF-Chem
172 (Benavente et al., 2023). We artificially increase simulated AOD by 0.04 globally to address this
173 poorly understood systematic bias that, although minor, is useful for the representation of η

174 (PWMD reduced from 20.6 $\mu\text{g}/\text{m}^3$ to 1.9 $\mu\text{g}/\text{m}^3$). $\text{PM}_{2.5}$ is calculated as the sum of each component
175 at 35% RH to align with common measurement protocols.

176 **2.5 Population**

177 Global population information is obtained from the Gridded Population of the World provided by
178 the NASA Socioeconomic Data and Applications Center (Center for International Earth Science
179 Information Network, 2018).

180 **2.6 Sensitivity Tests with Globally Uniform Parameters**

181 We conduct sensitivity tests of factors affecting the spatial variation of η , with a focus on aerosol
182 composition and aerosol vertical profile. To understand the relative importance of these factors,
183 we impose a constant for each factor and simulate the corresponding η . The difference between
184 the test scenario and the base scenario reflects the change due to variation of the factor. We use
185 the global population-weighted mean (PWM) and population-weighted mean difference (PWMD)
186 to summarize changes with a focus on relevance to population exposure:

$$X_{PWM} = \frac{\sum_j \sum_i P_{i,j} X_{i,j}}{\sum_j \sum_i P_{i,j}}$$

187

$$PWMD = \frac{\sum_j \sum_i P_{i,j} |X_{i,j} - Y_{i,j}|}{\sum_j \sum_i P_{i,j}}$$

188 where i and j are grid box identifiers. X and Y could be any variable of interest. $|X_{i,j} - Y_{i,j}|$ is the
189 absolute value of their difference. P represents population density in each grid box.

190 The first test imposes globally uniform aerosol chemical composition calculated as the global
191 PWM aerosol component fraction ($F_{k,s,PWM}$):

$$F_{k,s,PWM} = \frac{\sum_j \sum_i P_{i,j} F_{i,j,k,s}}{\sum_j \sum_i P_{i,j}}$$

192 where i , j , and k are grid box identifiers along latitude, longitude, and vertical layer. F_s is the
193 fraction of aerosol component s in total aerosol mass. This test keeps the total columnar aerosol
194 mass and aerosol vertical profile unchanged.

195 The second test imposes a globally uniform aerosol vertical profile calculated as the PWM column
196 relative vertical profile ($R_{k,s,PWM}$):

$$R_{k,s,PWM} = \frac{\sum_j \sum_i P_{i,j} R_{i,j,k,s}}{\sum_j \sum_i P_{i,j}}$$

197 where $R_{i,j,k,s}$ is the relative dry mass ratio compared to the surface. The total mass loading and
198 relative chemical composition are unchanged.

199 We analyze global and regional variations of η , as well as that for the driving factors. The definition
200 of each region used in this study is summarized in Figure A3.

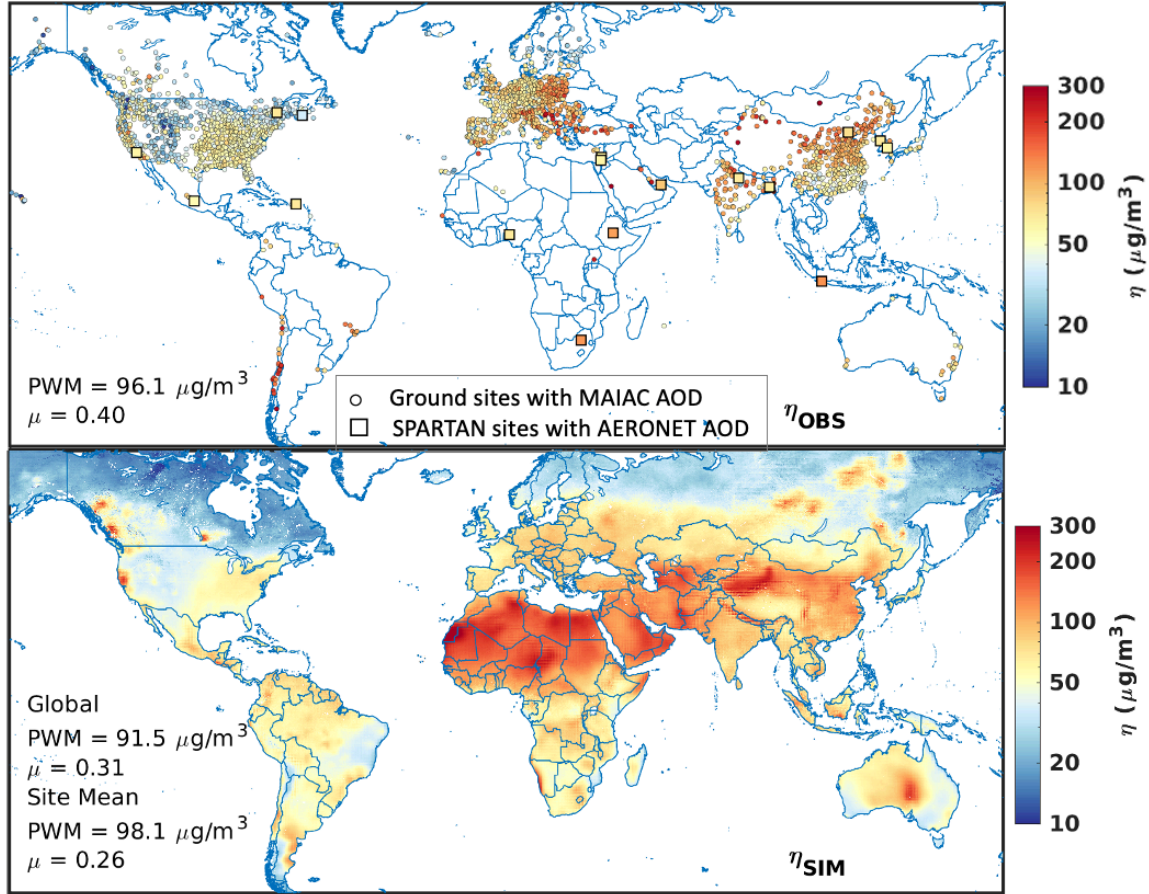
201 **3 Results and Discussion**

202 **3.1 Global Spatial Pattern of η**

203 The top panel of Figure 1 shows the observationally based annual mean η , inferred from the ratio
204 of ground-measured $PM_{2.5}$ to MAIAC AOD. Measurements are most dense in North America,
205 Europe, and East Asia. The annual mean η varies substantially, from 7.8 $\mu\text{g}/\text{m}^3$ in Hawaii to 504
206 $\mu\text{g}/\text{m}^3$ in Mongolia, with a PWM of 96.1 $\mu\text{g}/\text{m}^3$. Higher PWM η of 196 $\mu\text{g}/\text{m}^3$ to 154 $\mu\text{g}/\text{m}^3$ exist
207 over desert regions such as Africa and West Asia, followed by PWM η of 97 $\mu\text{g}/\text{m}^3$ to 119 $\mu\text{g}/\text{m}^3$
208 over regions strongly influenced by anthropogenic aerosols, such as East Asia and South Asia
209 (Figure A4 and Table A1). Over North America, η is around 60 $\mu\text{g}/\text{m}^3$ in the east and in California,
210 which is more than double that in the Rockies, driven by the spatial pattern of surface $PM_{2.5}$ (Figure
211 A4). The PWM η in North America of 59.8 $\mu\text{g}/\text{m}^3$ is about 30% lower than the global PWM. The
212 η pattern found here is similar to that reported by Jin et al. (2020) for the U.S. In Europe, η also
213 varies noticeably between the east and the west, driven by the spatial pattern of surface $PM_{2.5}$, as
214 $PM_{2.5}$ increases by 60% from west to east while AOD increases by only 8%. The PWM η in Europe
215 is 92.3 $\mu\text{g}/\text{m}^3$, slightly lower than the global PWM. In Asia, measured η is concentrated in China
216 and India. In China, the η spatial pattern shows a clear distinction between the northern and
217 southern regions, driven by the higher AOD in the south (Figure A5), where relative humidity is
218 high. A similar η spatial pattern and a negative correlation between η and RH are reported by Yang
219 et al. (2019). In India, η is highest in the northwest, with a PWM η of 129 $\mu\text{g}/\text{m}^3$, and decreases to
220 about 80 $\mu\text{g}/\text{m}^3$ toward the east and the south. Both $PM_{2.5}$ and AOD follow the same spatial pattern,

221 while $PM_{2.5}$ exhibits a stronger decreasing tendency (Figure A4 and Figure A5). PWM η in Asia
222 is $102 \mu\text{g}/\text{m}^3$, the highest among the populous regions and 6.0% higher than the global PWM.
223 Globally, from west to east, η increases by about 70%, despite that both $PM_{2.5}$ and AOD increased
224 more than threefold (Figure A6). The coefficient of variation (standard deviation divided by mean)
225 in η is higher in Europe ($\mu = 0.31$) and Asia ($\mu = 0.36$), than North America ($\mu = 0.25$, Figure A6).

226 The bottom panel in Figure 1 shows the GCHP simulated η , the ratio between simulated 24-hour
227 mean surface $PM_{2.5}$ and simulated total column AOD at satellite overpass time. The simulation
228 generally reproduces the global observations of η with a tendency for high values in arid regions
229 influenced by dust and low values in regions distant from strong surface sources. The simulated
230 global PWM η is 2% higher than the observations ($98.1 \mu\text{g}/\text{m}^3$ vs. $96.1 \mu\text{g}/\text{m}^3$), mostly driven by
231 an overestimation in East Asia ($108 \mu\text{g}/\text{m}^3$ vs. $96.9 \mu\text{g}/\text{m}^3$), that reflects an overestimation of PWM
232 $PM_{2.5}$ ($43.3 \mu\text{g}/\text{m}^3$ vs. $38.0 \mu\text{g}/\text{m}^3$). The simulation generally reproduces the regional spatial pattern
233 in North America and Asia but underestimates the η variability in Europe as it overestimates η in
234 central Europe and underestimates η in Eastern Europe, due to positive bias in simulated $PM_{2.5}$ in
235 central Europe and positive bias in simulated AOD in Eastern Europe. Nonetheless, the PWM η
236 in Europe ($83.6 \mu\text{g}/\text{m}^3$) is within 9.4% of observations. Globally, there is overall consistency
237 between the simulated η and observed η , with a correlation of 0.59, resulting in a high degree of
238 consistency between geophysical $PM_{2.5}$ and measured $PM_{2.5}$ ($r = 0.89$, Figure A6). Evaluation of
239 the simulation of $PM_{2.5}$ chemical composition versus ground-based measurements reveals a high
240 degree of consistency (Figure A2) that supports their further assessment of the factors affecting η .



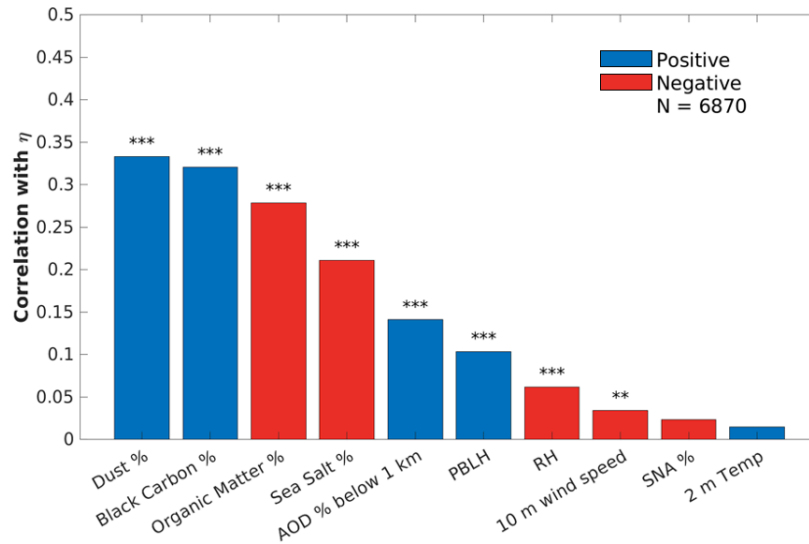
241

242 Figure 1. Observed (top) and simulated (bottom) annual mean η for 2019. Circles represent ground
 243 measurement sites from regional networks or the World Health Organization. Squares represent co-
 244 located ground measured $\text{PM}_{2.5}$ from SPARTAN and AOD from AERONET. PWM = population-
 245 weighted mean, μ = coefficient of variation (standard deviation divided by mean).

246 We explore the dominant driving factors for η spatial variation by calculating the spatial
 247 correlation between each candidate factor and the observation-based η . Candidate factors
 248 examined include meteorological fields (MERRA-2), aerosol vertical profile, and aerosol
 249 composition as collected from the GCHP simulation or SPARTAN. Meteorological fields include
 250 those commonly considered to represent the temporal variation in η , such as PBLH, RH at 700
 251 hPa, wind speed at 10 m, and temperature at 2 m (Chu et al., 2015; Damascena et al., 2021; He et
 252 al., 2021; Yang et al., 2019). The aerosol vertical profile is represented as the AOD fraction below
 253 1 km (AOD % below 1 km). Aerosol composition includes SNA, OM, dust, black carbon, and sea
 254 salt, all represented as the fractional contributions (%) to surface $\text{PM}_{2.5}$. Figure 2 shows the spatial

255 correlation of annual mean factors versus observation-based η . Aerosol components, particularly
256 those with strong primary sources (dust, OM, and black carbon), exhibit the strongest correlations
257 (>0.27) with observationally based η . Significant positive correlations are found for mineral dust
258 and black carbon, both of which are non- or weakly-hygroscopic. Significant negative correlations
259 are found for organic matter and sea salt, reflecting a weak connection between surface
260 concentrations and AOD aloft. Processes are further discussed in sections 3.2 and 3.4. The aerosol
261 vertical profile exhibits a moderate correlation with η (0.14), which is notably higher than any
262 meteorological factors (≤ 0.10). Ground-based data from SPARTAN and AERONET corroborate
263 the correlation between aerosol composition and η (Figure A7). We thus focus further analysis in
264 Sections 3.2-3.4 on the two main drivers in η : aerosol composition and aerosol vertical profile.

265 The drivers of spatial variation in η found here differ from that for temporal variation of η in prior
266 work (e.g. He et al. 2021), reflecting the different processes involved. Meteorological parameters
267 drive short-term variability in the aerosol vertical profile, such as day-to-day variation in mixed
268 layer depth or in advection from a point source. In contrast, the spatial variation in annual mean η
269 reflects the spatial variation in processes affecting the long-term relation of surface $PM_{2.5}$ at
270 controlled RH of 35% with AOD at ambient RH. Aerosol composition and the aerosol vertical
271 profile reflect spatial variation in aerosol hygroscopicity, mass extinction efficiency, and sources.
272 The following sections explore how aerosol composition and aerosol vertical profile vary globally
273 and examine how they affect the spatial pattern of η by conducting two sensitivity tests. In each
274 sensitivity test, we replace the spatial variability of a factor with a globally uniform value. The
275 variability of aerosol composition and aerosol vertical profile are discussed in sections 3.2 and 3.3,
276 respectively. The sensitivity test results are discussed in section 3.4.



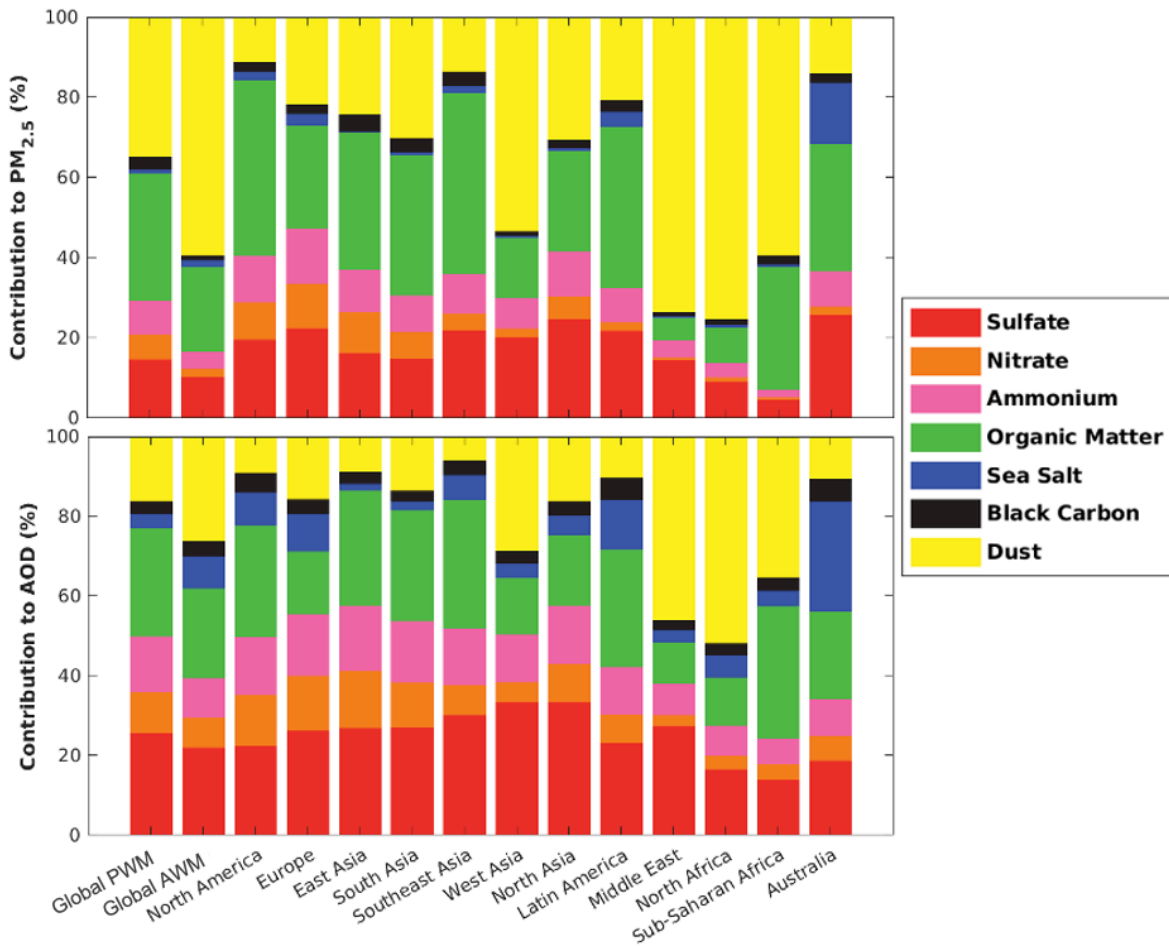
277

278 Figure 2. Spatial correlation between annual mean modeled parameters and observationally-based η . Blue
 279 bars indicate positive correlations. Red bars indicate negative correlations. Stars above each bar indicate
 280 the p-value associated with each correlation. ‘***’ indicates the p-value is lower than 0.001 and ‘**’
 281 indicates lower than 0.01.

282 3.2 Spatial Variability in Aerosol Composition

283 Figure 3 shows the simulated PWM aerosol composition globally and regionally, as well as the
 284 global area-weighted mean (AWM). The top panel shows the compositional contribution to $PM_{2.5}$.
 285 Globally, dust is the leading PWM $PM_{2.5}$ component (34.7%), followed by OM (31.9%) and SNA
 286 (29.3%). The bottom panel shows the compositional contribution to AOD. PWM AOD
 287 composition is more evenly distributed, with more contribution from SNA (49.9%), followed by
 288 OM (27.2%) and dust (16.1%). Overall, more hygroscopic aerosols such as SNA tend to contribute
 289 a larger fraction of AOD which is at ambient RH, while less hygroscopic aerosols, such as mineral
 290 dust tend to contribute a larger fraction of $PM_{2.5}$ which is at controlled RH of 35%. The AWM
 291 $PM_{2.5}$ and AOD composition exhibit weaker contributions from SNA, primarily reflecting a larger
 292 contribution from dust in remote regions than in more densely populated areas. Over populous
 293 regions such as North America, Europe, and Southeast Asia, there are greater SNA and OM
 294 fractions than the global mean (Figure 3). Arid regions, such as West Asia, the Middle East, North
 295 Africa, and Sub-Saharan Africa, have large fractions of non-hygroscopic mineral dust that (1)
 296 reduce aerosol mass extinction efficiency, yielding less AOD per unit mass, and (2) are unaffected

297 by the controlled RH of $PM_{2.5}$. Both of these factors increase η in dusty regions compared with
 298 regions dominated by hygroscopic SNA aerosols.

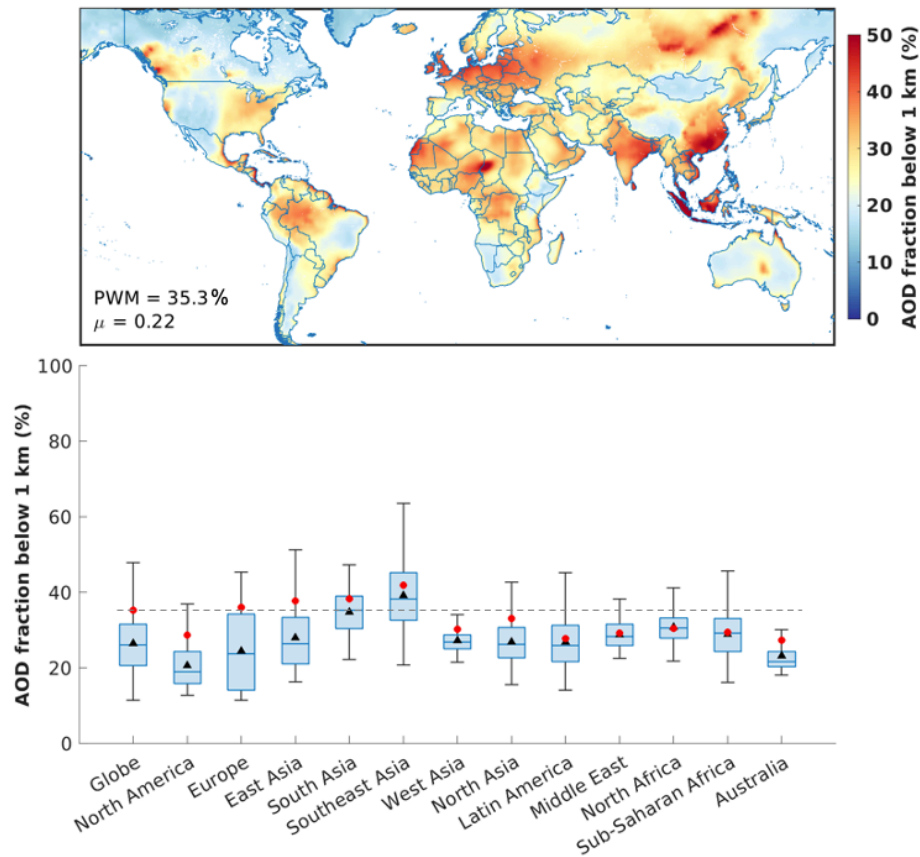


299
 300 Figure 3. Global and regional PWM contributions of aerosol composition to surface $PM_{2.5}$ (top) and AOD
 301 (bottom). The global area-weighted mean (AWM) over land is also included as the second column.

302 3.3 Spatial Variability in Aerosol Vertical Profile

303 Figure 4 shows the AOD fraction below 1 km in the GEOS-Chem simulation. Globally, 35.3% of
 304 the PWM AOD is below 1 km. The PWM value is greater than the AWM value since populated
 305 areas tend to have more surface emissions of particles and precursors. Over North America, Europe,
 306 and East Asia, the PWM surface AOD fractions are much higher than the medians and AWM,
 307 indicating high spatial heterogeneity between urban and remote areas. Europe exhibits the highest
 308 variation and the largest discrepancy between PWM and AWM, reflecting the largest spatial
 309 heterogeneity in aerosol vertical profile, driven by influences from regional pollution, marine

310 aerosols, and transported dust (Zhao et al., 2018). Southeast Asia has the highest surface AOD
 311 fraction and a large variation. Local sources, long-range transported dust, and the influence of
 312 trade winds all contribute to the unique spatial variation in aerosol vertical profile in this region
 313 (Banerjee et al., 2021; Nguyen et al., 2019). Globally, PWM values exhibit less variation than
 314 AWM, indicating moderate variation in aerosol profile across populous areas.



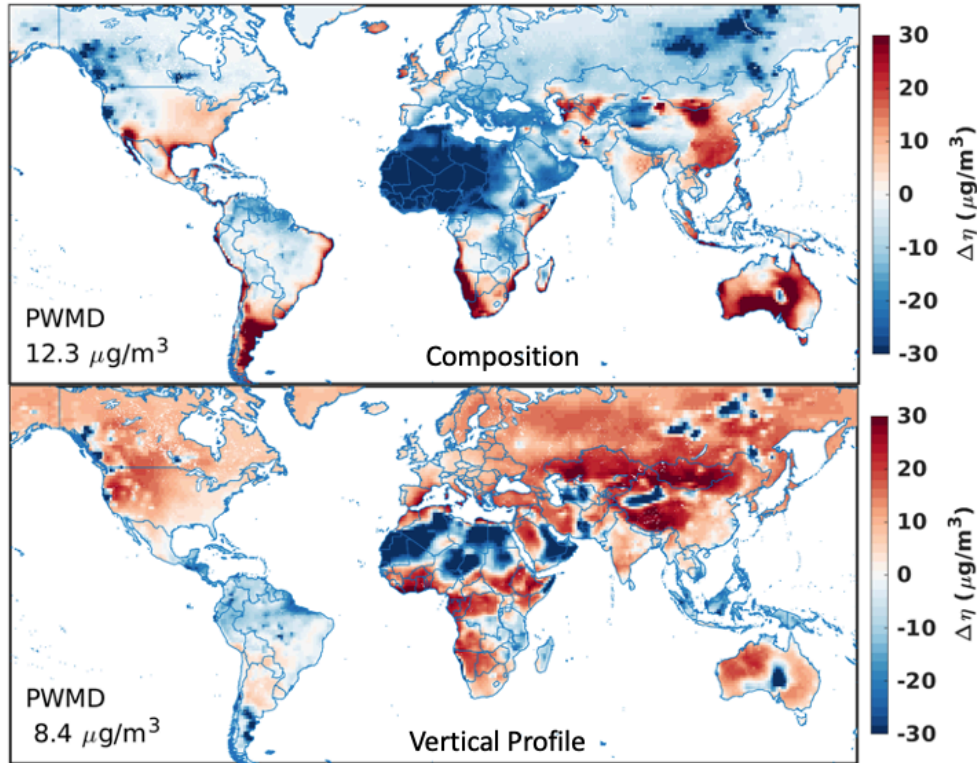
315
 316 Figure 4. (Top) Map of AOD fraction below 1 km. (Bottom) Global and regional statistics for AOD
 317 fraction below 1 km. Black triangles show the area-weighted mean. Red circles show the PWM. The line
 318 inside each box is the sample median. Each box's top and bottom edges are the 75 and 25 quartiles,
 319 respectively. Vertical bars are the maximum and minimum values within 1.5 times the interquartile range.
 320 The dashed line indicates global PWM.

321 3.4 Sensitivity Tests with Globally Uniform Parameters

322 Figure 5 shows the global changes in the spatial variation in η due to variations in aerosol chemical
 323 composition (top) and aerosol vertical profile (bottom), the two main drivers found in Figure 2.

324 Globally, neglect of spatial variation in aerosol composition induces a $12.3 \mu\text{g}/\text{m}^3$ PWMD in η
325 spatial variation. Both $\text{PM}_{2.5}$ and AOD are strongly affected by aerosol composition, following a
326 similar spatial pattern (Figure A8). Over mid- and low-latitude areas, the change in AOD is
327 stronger than in $\text{PM}_{2.5}$, since AOD at ambient RH is more sensitive to hygroscopicity changes.
328 This yields the opposite pattern in the η . Neglect of spatial variation in chemical composition
329 reduces η over North Africa and the Middle East, desert regions where aerosols contain more
330 weakly hygroscopic components such as mineral dust, compared to populous areas, which contain
331 more secondary inorganic aerosol (Figure 3). For smaller deserts in the Southwest U.S., Argentina,
332 and Southwest Africa, the dust fractions of surface aerosols are higher than the global mean (36%,
333 76%, and 49%, respectively), but the dust fraction for AOD is similar to the global mean (15%,
334 25%, and 14%, respectively). Therefore, neglect of the spatial variation of chemical composition
335 increases η over these small deserts by increasing the fraction of hygroscopic components in $\text{PM}_{2.5}$
336 and leaving AOD almost unchanged (Figure A8). Neglect of spatial variation in chemical
337 composition also reduces η over the boreal forests, where surface aerosols are more hygroscopic
338 compared to populous areas and show strong changes, while less so for column aerosol (Figure
339 A8). Neglect of spatial variation in chemical composition increases η over the eastern U.S. and
340 eastern China, where $\text{PM}_{2.5}$ contains more hygroscopic SNA and less dust than the global mean. It
341 also increases η in coastal regions where aerosol contains more hygroscopic sea salt than the global
342 mean.

343 Neglect of spatial variation in the aerosol vertical profile induces an $8.4 \mu\text{g}/\text{m}^3$ PWMD in η spatial
344 variation (Figure 5), following the spatial pattern of the change in surface $\text{PM}_{2.5}$ (Figure A9). The
345 most apparent feature is an increase in η throughout the remote northern hemisphere, driven by an
346 increased aerosol fraction near the surface where the fraction is normally small (Figure 4). The
347 uniform aerosol vertical profile decreases η over northern Africa and biomass burning regions of
348 the boreal forests, the Amazon, and Indonesia, driven by a decreased aerosol fraction near the
349 surface in regions where that fraction is normally high.



350

351 Figure 5. Changes in η (test -base) for each sensitivity test. In the first test, a global PWM aerosol
 352 composition replaces the actual composition (top). In the second test, a global PWM aerosol profile
 353 replaces the actual profiles (bottom). Numbers inset indicate population-weighted mean difference
 354 (PWMD).

355 **Conclusion**

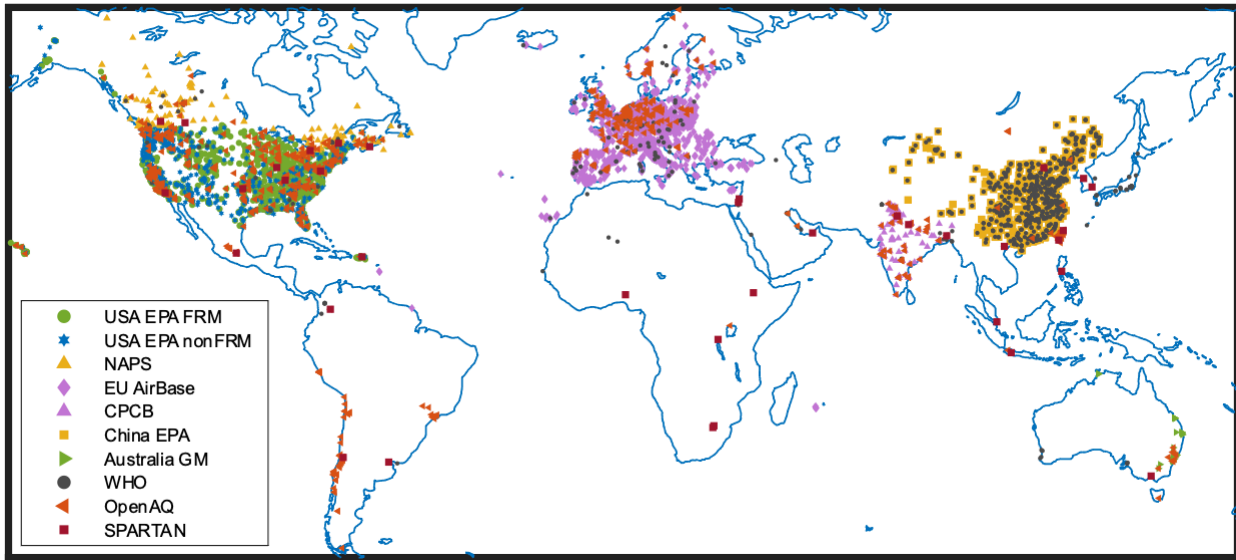
356 Understanding the global variation of the $\text{PM}_{2.5}$ and AOD relationship (η) offers insight into the
 357 geophysical inference of $\text{PM}_{2.5}$ from satellite AOD observations. We collected ground-based $\text{PM}_{2.5}$
 358 measurements from 6,870 sites and MODIS MAIAC satellite AOD throughout the year 2019 to
 359 obtain, for the first time, a global scale observationally based η map. Observed annual mean η
 360 ranges from $7.8 \mu\text{g}/\text{m}^3$ in Hawaii to $504 \mu\text{g}/\text{m}^3$ in Mongolia. We observed enhanced η of $196 \mu\text{g}/\text{m}^3$
 361 to $154 \mu\text{g}/\text{m}^3$ over arid regions such as Africa and West Asia, due to their low aerosol extinction
 362 efficiency. Moderate η of $97 \mu\text{g}/\text{m}^3$ to $119 \mu\text{g}/\text{m}^3$ was found in industrial areas such as East Asia
 363 and South Asia, where anthropogenic emissions increase the near-surface $\text{PM}_{2.5}$ concentrations.
 364 Over remote areas, low η ($< 50 \mu\text{g}/\text{m}^3$) was usually observed.

365 We simulated the global annual mean η with the GEOS-Chem chemical transport model in its high
366 performance configuration (GCHP). The simulation generally represented observed η with PWM
367 within 3% ($98.1 \mu\text{g}/\text{m}^3$ vs $96.1 \mu\text{g}/\text{m}^3$) and a correlation of 0.59 over the 6,780 measurement sites.
368 We examined the correlation between simulation and measurements to identify the two most
369 impactful drivers for η spatial variation - aerosol composition and aerosol vertical profile, both of
370 which strongly affect the annual mean relation of columnar AOD at ambient RH with surface
371 $\text{PM}_{2.5}$ at controlled RH of 35%. We subsequently conducted sensitivity tests by eliminating the
372 spatial variation of each of the two drivers and quantified the impact on η spatial variability.
373 Imposing a globally uniform aerosol composition led to pronounced changes (PWMD = 12.3
374 $\mu\text{g}/\text{m}^3$), reflecting how changes in aerosol composition affect both AOD and surface $\text{PM}_{2.5}$, due to
375 the effects of aerosol hygroscopicity on both quantities. Imposing a globally uniform aerosol
376 vertical profile had a moderate effect (PWMD = $8.4 \mu\text{g}/\text{m}^3$), reflecting changes in the fraction of
377 aerosol near the surface.

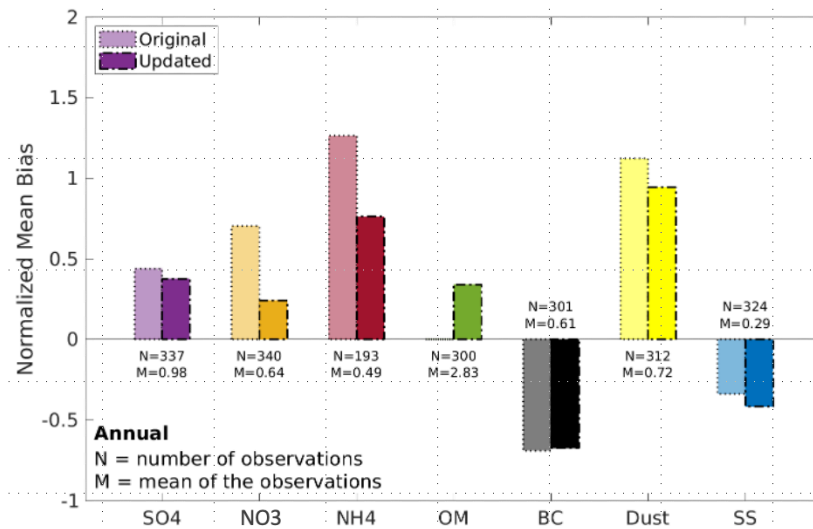
378 These findings motivate additional efforts to develop the simulation of aerosol composition and
379 aerosol vertical profile. Promising avenues include: (1) enhancing global long-term measurements
380 of $\text{PM}_{2.5}$ chemical composition to evaluate and improve simulations, (2) exploiting new and
381 emerging information about aerosol type from satellite remote sensing (e.g. PACE, MAIA), (3)
382 advancing simulations at finer spatial resolution to better represent processes affecting aerosol
383 composition and vertical profile, (4) leveraging aircraft, lidar, and collected AOD-to- $\text{PM}_{2.5}$
384 measurements for constraints on the vertical profile, and (5) exploiting nascent capabilities in
385 applying satellite remote sensing (e.g. TROPOMI, TEMPO, GEMS) for top-down constraints on
386 emissions that affect aerosol composition.

387

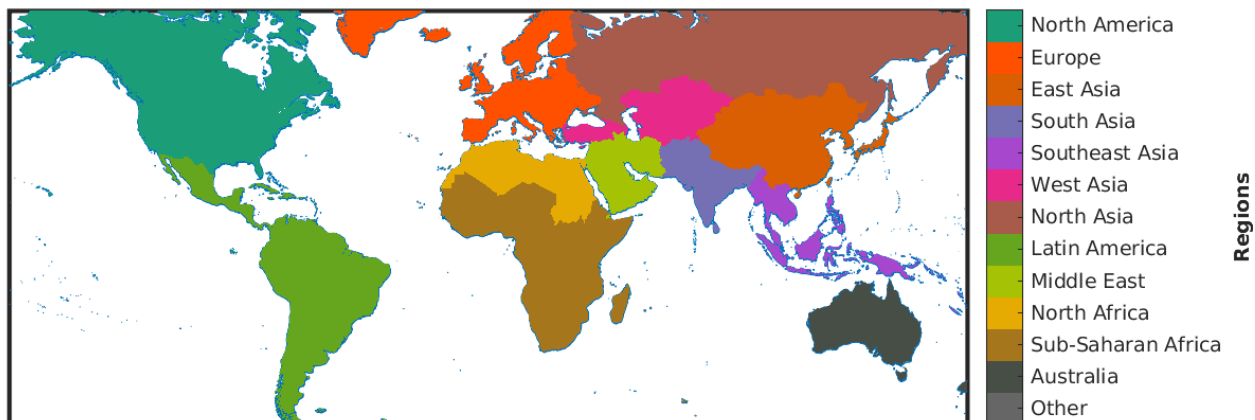
388 **Appendix**



389
390 Figure A1. PM_{2.5} measurement sites from publicly available networks.

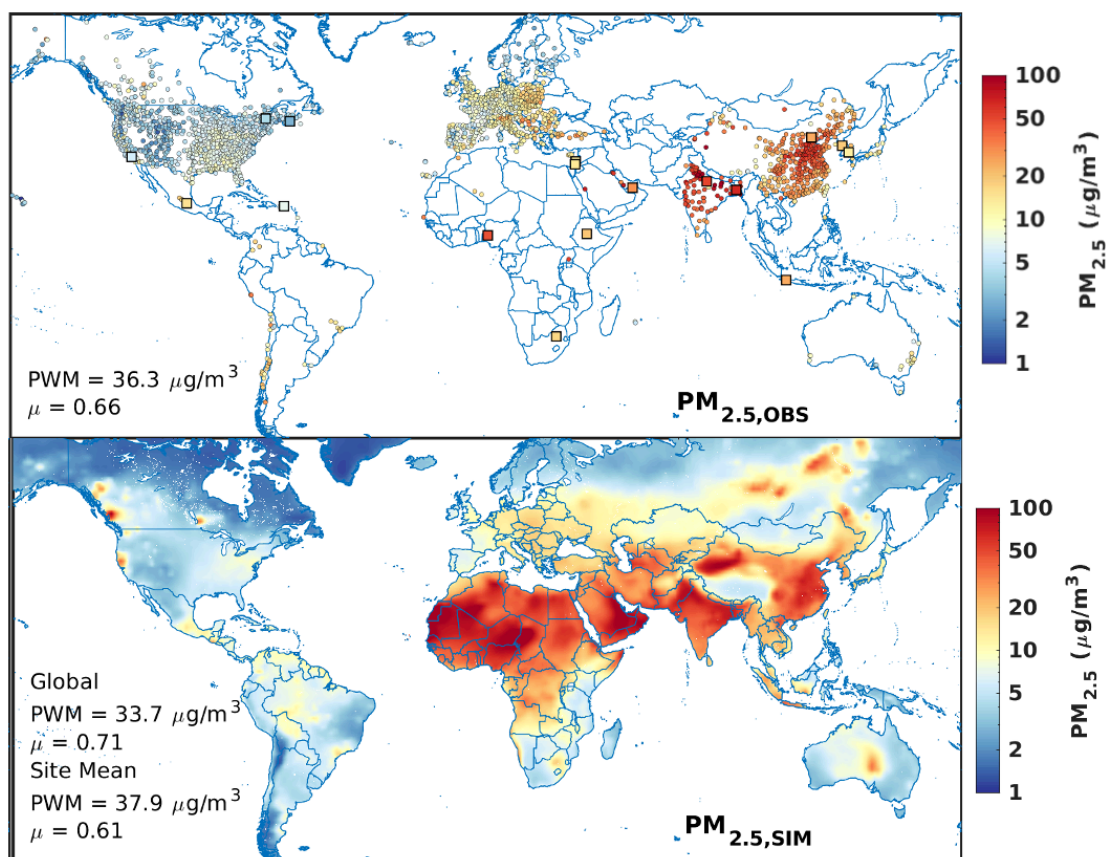


391
392 Figure A2. Normalized mean bias (NMB) between simulated PM_{2.5} chemical composition and ground
393 measurements from CSN, IMPROVE, EBAS, and SPARTAN. The original simulation is the out-of-box
394 version of GCHP v13.4.0, the updated simulation includes adjustments such as GFED4.1s emission at daily
395 scale, diel variation and vertical distribution of anthropogenic emissions, and 50% reduction in nitrate
396 concentration.



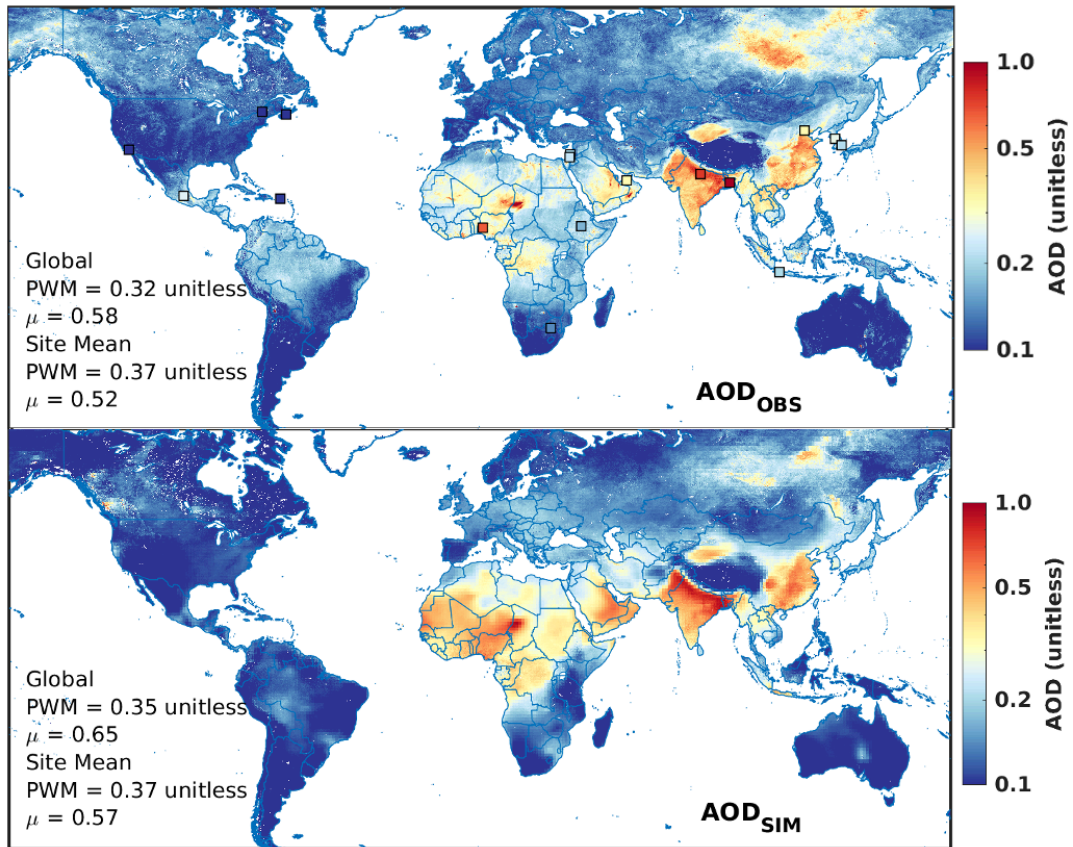
397

398 Figure A3. Region definition.



399

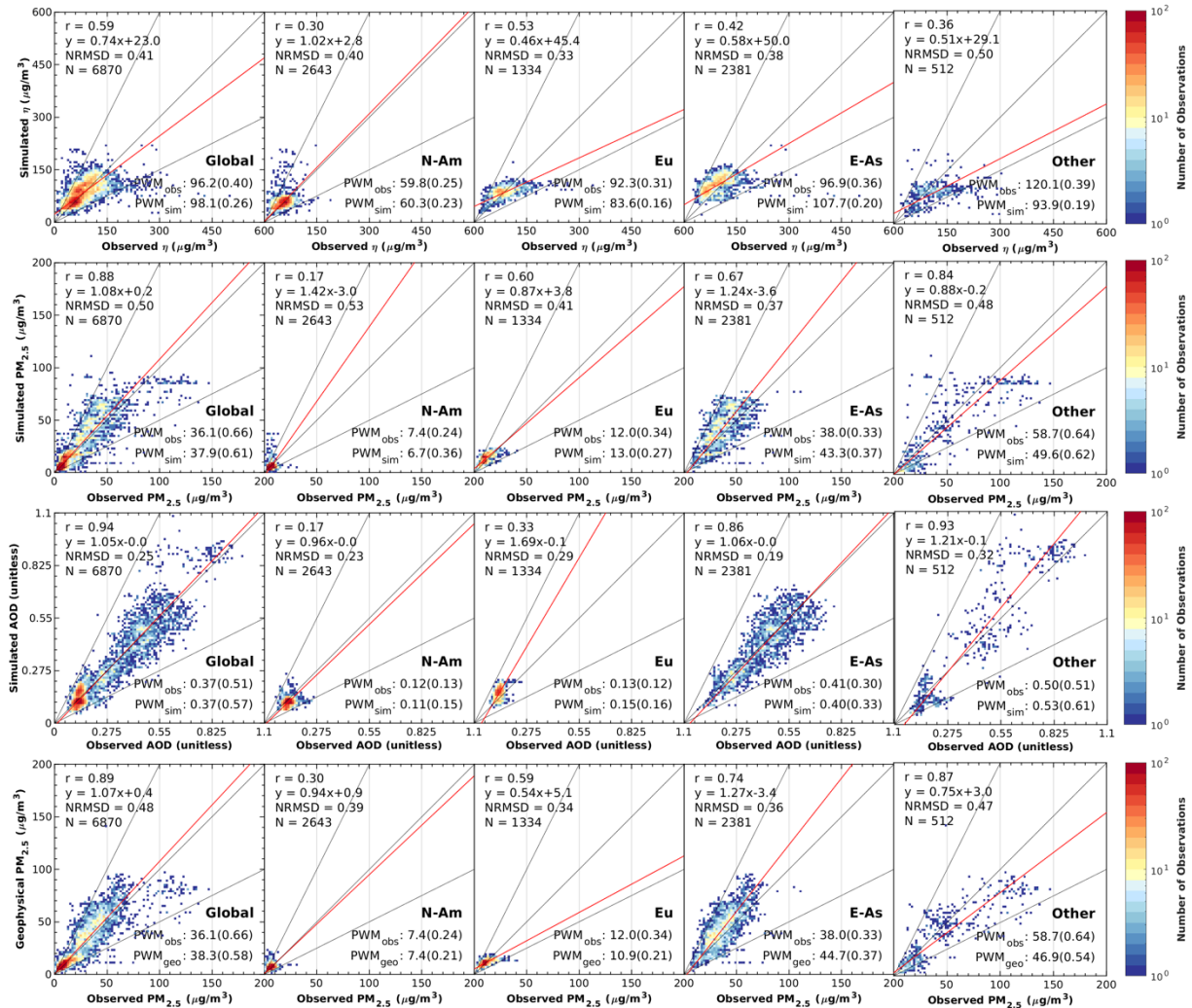
400 Figure A4. Observed (top) and simulated (bottom) annual mean $\text{PM}_{2.5}$ for 2019. Circles represent
 401 measurement sites from regional networks or reported by the WHO. Squares represent measured $\text{PM}_{2.5}$
 402 from SPARTAN. PWM = population-weighted mean, μ = coefficient of variation.



403

404 Figure A5. Satellite retrieved (top) and GCHP simulated (bottom) annual mean AOD for 2019. Squares
 405 represent ground-measured AOD from AERONET. PWM = population-weighted mean, μ = coefficient of
 406 variation.

407



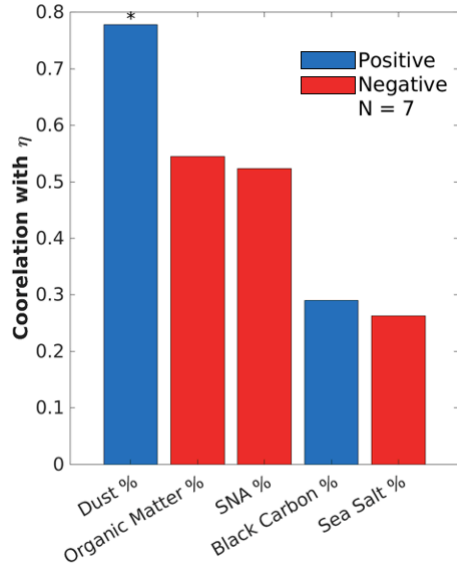
408

409 Figure A6. Scatter plots of simulated and observed η (top row), simulated and ground measured $PM_{2.5}$
 410 (second row), simulated and MAIAC AOD (third row), and geophysical and observed $PM_{2.5}$ (bottom
 411 row). The red line shows the line of best fit using Reduced Major Axis Linear Regression. Insets on the
 412 top left show the coefficient of determination (R^2), line of best fit, normalized root mean square deviation
 413 (NRMSD), and total number of data points (N). The bottom right insets show the population-weighted
 414 mean of observed, simulated, or geophysical estimation of each dataset, coefficients of variation are
 415 bracketed. Detailed regional mean and coefficients of variation for other regions can be found in Table
 416 A1.

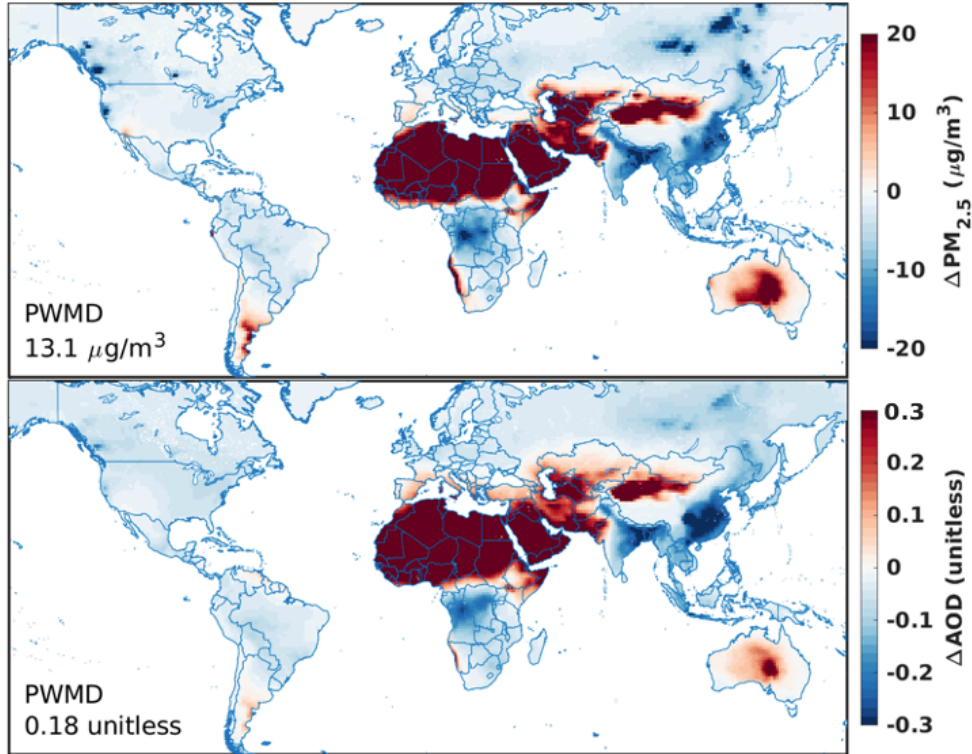
417 Table A1. Regional population-weighted mean η , $\text{PM}_{2.5}$, and AOD from both observation and
 418 simulations. Geophysical $\text{PM}_{2.5}$ is also included. Coefficients of variation are bracketed. Regional mean
 419 and coefficients of variation for North America, Europe, and East Asia can be found in Figure A6.

Region		South Asia	Southeast Asia	West Asia	Latin America	Middle East	North Africa	Sub-Saharan Africa	Australia
Number of sites		220	5	43	2	142	32	3	6
η [$\mu\text{g}/\text{m}^3$]	Observed	119.5 (0.36)	111.4 (0.21)	154.0 (0.23)	72.0 (0.29)	117.5 (0.51)	135.0 (0.32)	196.0 (0.01)	187.8 (0.34)
	Simulated	95.0 (0.14)	93.8 (0.18)	93.4 (0.03)	74.1 (0.04)	86.6 (0.18)	135.8 (0.19)	105.9 (0.01)	128.4 (0.54)
$\text{PM}_{2.5}$ [$\mu\text{g}/\text{m}^3$]	Observed	75.7 (0.45)	40.6 (0.26)	22.0 (0.21)	12.0 (0.23)	20.4 (0.36)	32.2 (0.53)	24.0 (0.00)	46.3 (0.29)
	Simulated	64.9 (0.37)	38.1 (0.23)	20.8 (0.08)	20.9 (0.06)	10.1 (0.30)	47.2 (0.52)	16.7 (0.03)	56.6 (0.87)
	Geo-physical	59.9 (0.31)	36.1 (0.43)	13.9 (0.08)	12.4 (0.08)	17.6 (0.39)	33.0 (0.40)	12.9 (0.03)	37.0 (0.99)
AOD [unitless]	Observed	0.63 (0.29)	0.38 (0.30)	0.14 (0.08)	0.17 (0.03)	0.20 (0.32)	0.23 (0.30)	0.12 (0.01)	0.27 (0.52)
	Simulated	0.69 (0.36)	0.40 (0.12)	0.22 (0.09)	0.28 (0.02)	0.21 (0.23)	0.33 (0.34)	0.16 (0.01)	0.37 (0.47)

420

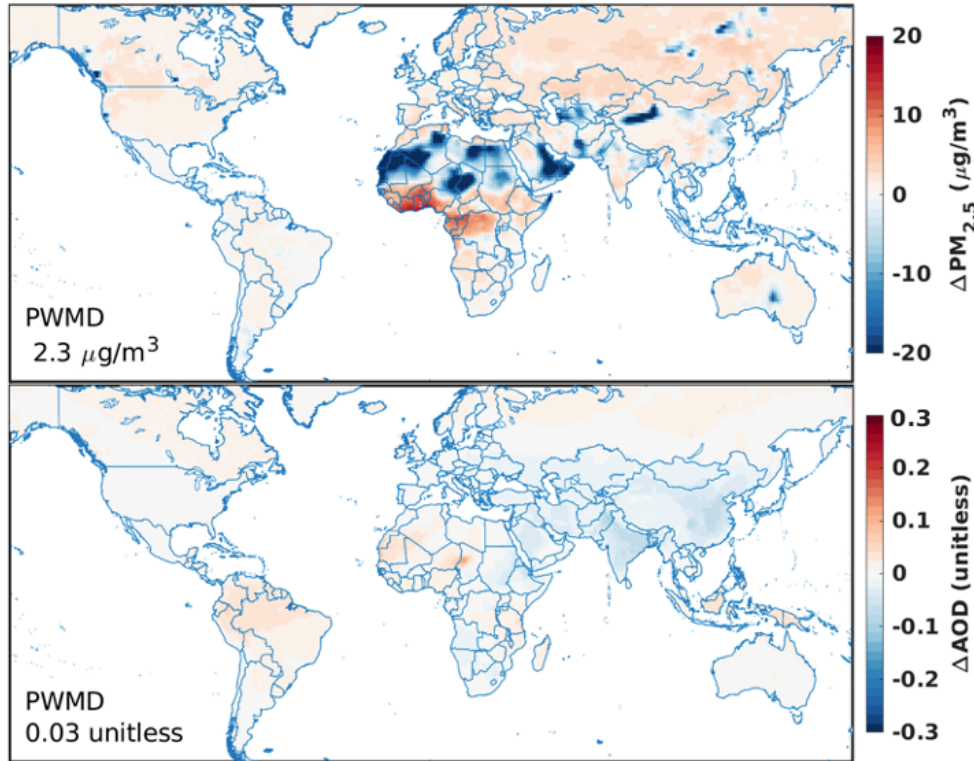


421
 422 Figure A7. Correlation with η of ground-measured aerosol fractional composition from SPARTAN.
 423 Organic matter is inferred through residual (Snider et al., 2016). Blue bars indicate positive correlations.
 424 Red bars indicate negative correlations. Stars above each bar indicate the p-value associated with each
 425 correlation. ‘***’ means the p-value is lower than 0.001, ‘**’ means lower than 0.01, and ‘*’ means
 426 lower than 0.5.



427

428 Figure A8. Changes in PM_{2.5} (top) and AOD (bottom) (test - base) when imposing a global PWM aerosol
429 composition.



430

431 Figure A9. Changes in PM_{2.5} (top) and AOD (bottom) (test - base) when imposing a global PWM aerosol
 432 profile.

433 *Data availability.* GEOS-Chem in its high-performance configuration version 13.4.0 can be
 434 downloaded at <https://zenodo.org/records/6564711>.

435 *Author contributions.* HZ and RVM designed the study. HZ performed the data analysis and model
 436 simulation with contributions from AvD, CL, YL, DZ, JM, MH & IS. AvD contributed to the
 437 compiled the MAIAC AOD dataset and ground-based observation datasets for PM_{2.5}. AL
 438 contributed to the original MAIAC AOD dataset. CRO and XL contributed to the SPARTAN data
 439 utilization and analysis. The manuscript was written by HZ and RVM with contributions from all
 440 authors.

441 *Competing interests.* The authors declare no competing financial interest.

442 *Acknowledgment.* This work was supported by NASA Grant 80NSSC22K0200. We thank Dr. Mi
 443 Zhou from Princeton University for providing ground based PM_{2.5} data over India.

444

445 Reference

- 446 Amos, H. M., Jacob, D. J., Holmes, C. D., Fisher, J. A., Wang, Q., Yantosca, R. M., Corbitt, E. S.,
447 Galarneau, E., Rutter, A. P., Gustin, M. S., Steffen, A., Schauer, J. J., Graydon, J. A., St Louis, V.
448 L., Talbot, R. W., Edgerton, E. S., Zhang, Y., and Sunderland, E. M.: Gas-particle partitioning of
449 atmospheric Hg(II) and its effect on global mercury deposition, *Atmospheric Chemistry and*
450 *Physics*, 12, 591–603, <https://doi.org/10.5194/acp-12-591-2012>, 2012.
- 451 Banerjee, T., Shitole, A. S., Mhawish, A., Anand, A., Ranjan, R., Khan, M. F., Srithawirat, T.,
452 Latif, M. T., and Mall, R. K.: Aerosol Climatology Over South and Southeast Asia: Aerosol Types,
453 Vertical Profile, and Source Fields, *Journal of Geophysical Research: Atmospheres*, 126,
454 e2020JD033554, <https://doi.org/10.1029/2020JD033554>, 2021.
- 455 Benavente, N. R., Vara-Vela, A. L., Nascimento, J. P., Acuna, J. R., Damascena, A. S., de Fatima
456 Andrade, M., and Yamasoe, M. A.: Air quality simulation with WRF-Chem over southeastern
457 Brazil, part I: Model description and evaluation using ground-based and satellite data, *Urban*
458 *Climate*, 52, 101703, <https://doi.org/10.1016/j.uclim.2023.101703>, 2023.
- 459 Bieser, J., Aulinger, A., Matthias, V., Quante, M., and Denier Van Der Gon, H. A. C.: Vertical
460 emission profiles for Europe based on plume rise calculations, *Environmental Pollution*, 159,
461 2935–2946, <https://doi.org/10.1016/J.ENVPOL.2011.04.030>, 2011.
- 462 Brauer, M., Roth, G. A., Aravkin, A. Y., Zheng, P., Abate, K. H., Abate, Y. H., Abbafati, C.,
463 Abbasgholizadeh, R., Abbasi, M. A., Abbasian, M., Abbasifard, M., Abbasi-Kangevari, M.,
464 ElHafeez, S. A., Abd-Elsalam, S., Abdi, P., Abdollahi, M., Abdoun, M., Abdulah, D. M.,
465 Abdullahi, A., Abebe, M., Abedi, A., Abedi, A., Abegaz, T. M., Zuñiga, R. A. A., Abiodun, O.,
466 Abiso, T. L., Aboagye, R. G., Abolhassani, H., Abouzid, M., Aboye, G. B., Abreu, L. G., Abualruz,
467 H., Abubakar, B., Abu-Gharbieh, E., Abukhadajah, H. J. J., Aburuz, S., Abu-Zaid, A., Adane, M.
468 M., Addo, I. Y., Addolorato, G., Adedoyin, R. A., Adekanmbi, V., Aden, B., Adetunji, J. B.,
469 Adeyeoluwa, T. E., Adha, R., Adibi, A., Adnani, Q. E. S., Adzighbli, L. A., Afolabi, A. A., Afolabi,
470 R. F., Afshin, A., Afyouni, S., Afzal, M. S., Afzal, S., Agampodi, S. B., Agbozo, F., Aghamiri, S.,
471 Agodi, A., Agrawal, A., Agyemang-Duah, W., Ahinkorah, B. O., Ahmad, A., Ahmad, D., Ahmad,
472 F., Ahmad, N., Ahmad, S., Ahmad, T., Ahmed, A., Ahmed, A., Ahmed, A., Ahmed, L. A., Ahmed,
473 M. B., Ahmed, S., Ahmed, S. A., Ajami, M., Akalu, G. T., Akara, E. M., Akbarialiabad, H.,
474 Akhlaghi, S., Akinosoglou, K., Akinyemiju, T., Akkaif, M. A., Akkala, S., Akombi-Inyang, B.,
475 Awaidy, S. A., Hasan, S. M. A., Alahdab, F., AL-Ahdal, T. M. A., Alalalmeh, S. O., Alalwan, T.
476 A., Al-Aly, Z., Alam, K., Alam, N., Alanezi, F. M., Alanzi, T. M., Albakri, A., AlBataineh, M. T.,
477 Aldhaleei, W. A., et al.: Global burden and strength of evidence for 88 risk factors in 204 countries
478 and 811 subnational locations, 1990–2021: a systematic analysis for the Global Burden of Disease
479 Study 2021, *The Lancet*, 403, 2162–2203, [https://doi.org/10.1016/S0140-6736\(24\)00933-4](https://doi.org/10.1016/S0140-6736(24)00933-4), 2024.
- 480 Burnett, R., Chen, H., Szyszkowicz, M., Fann, N., Hubbell, B., Pope, C. A., Apte, J. S., Brauer,
481 M., Cohen, A., Weichenthal, S., Coggins, J., Di, Q., Brunekreef, B., Frostad, J., Lim, S. S., Kan,
482 H., Walker, K. D., Thurston, G. D., Hayes, R. B., Lim, C. C., Turner, M. C., Jerrett, M., Krewski,
483 D., Gapstur, S. M., Diver, W. R., Ostro, B., Goldberg, D., Crouse, D. L., Martin, R. V., Peters, P.,
484 Pinault, L., Tjepkema, M., Van Donkelaar, A., Villeneuve, P. J., Miller, A. B., Yin, P., Zhou, M.,

485 Wang, L., Janssen, N. A. H., Marra, M., Atkinson, R. W., Tsang, H., Thach, T. Q., Cannon, J. B.,
486 Allen, R. T., Hart, J. E., Laden, F., Cesaroni, G., Forastiere, F., Weinmayr, G., Jaensch, A., Nagel,
487 G., Concin, H., and Spadaro, J. V.: Global estimates of mortality associated with longterm
488 exposure to outdoor fine particulate matter, *Proceedings of the National Academy of Sciences of*
489 *the United States of America*, 115, 9592–9597, <https://doi.org/10.1073/pnas.1803222115>, 2018.

490 Canagaratna, M. R., Jimenez, J. L., Kroll, J. H., Chen, Q., Kessler, S. H., Massoli, P., Hildebrandt
491 Ruiz, L., Fortner, E., Williams, L. R., Wilson, K. R., Surratt, J. D., Donahue, N. M., Jayne, J. T.,
492 and Worsnop, D. R.: Elemental ratio measurements of organic compounds using aerosol mass
493 spectrometry: Characterization, improved calibration, and implications, *Atmospheric Chemistry*
494 *and Physics*, 15, 253–272, <https://doi.org/10.5194/acp-15-253-2015>, 2015.

495 Center for International Earth Science Information Network - CIESIN: Gridded Population of the
496 World, Version 4 (GPWv4): Population Density, Revision 11, 2018.

497 Christidis, T., Erickson, A. C., Pappin, A. J., Crouse, D. L., Pinault, L. L., Weichenthal, S. A.,
498 Brook, J. R., van Donkelaar, A., Hystad, P., Martin, R. V., Tjepkema, M., Burnett, R. T., and
499 Brauer, M.: Low concentrations of fine particle air pollution and mortality in the Canadian
500 Community Health Survey cohort, *Environmental Health*, 18, 84, [https://doi.org/10.1186/s12940-](https://doi.org/10.1186/s12940-019-0518-y)
501 [019-0518-y](https://doi.org/10.1186/s12940-019-0518-y), 2019.

502 Chu, D. A., Ferrare, R., Szykman, J., Lewis, J., Scarino, A., Hains, J., Burton, S., Chen, G., Tsai,
503 T., Hostetler, C., Hair, J., Holben, B., and Crawford, J.: Regional characteristics of the relationship
504 between columnar AOD and surface PM_{2.5}: Application of lidar aerosol extinction profiles over
505 Baltimore-Washington Corridor during DISCOVER-AQ, *Atmospheric Environment*, 101,
506 338e349-349, <https://doi.org/10.1016/j.atmosenv.2014.11.034>, 2015.

507 Cohen, A. J., Brauer, M., Burnett, R., Anderson, H. R., Frostad, J., Estep, K., Balakrishnan, K.,
508 Brunekreef, B., Dandona, L., Dandona, R., Feigin, V., Freedman, G., Hubbell, B., Jobling, A., Kan,
509 H., Knibbs, L., Liu, Y., Martin, R., Morawska, L., Pope, C. A., Shin, H., Straif, K., Shaddick, G.,
510 Thomas, M., van Dingenen, R., van Donkelaar, A., Vos, T., Murray, C. J. L., and Forouzanfar, M.
511 H.: Estimates and 25-year trends of the global burden of disease attributable to ambient air
512 pollution: an analysis of data from the Global Burden of Diseases Study 2015, *The Lancet*, 389,
513 1907–1918, [https://doi.org/10.1016/S0140-6736\(17\)30505-6](https://doi.org/10.1016/S0140-6736(17)30505-6), 2017.

514 Damascena, A. S., Yamasoe, M. A., Martins, V. S., Rosas, J., Benavente, N. R., Sánchez, M. P.,
515 Tanaka, N. I., and Saldiva, P. H. N.: Exploring the relationship between high-resolution aerosol
516 optical depth values and ground-level particulate matter concentrations in the Metropolitan Area
517 of São Paulo, *Atmospheric Environment*, 244, 117949,
518 <https://doi.org/10.1016/j.atmosenv.2020.117949>, 2021.

519 Di, Q., Kloog, I., Koutrakis, P., Lyapustin, A., Wang, Y., and Schwartz, J.: Assessing PM_{2.5}
520 Exposures with High Spatiotemporal Resolution across the Continental United States,
521 *Environmental Science and Technology*, 50, 4712–4721, <https://doi.org/10.1021/acs.est.5b06121>,
522 2016.

523 van Donkelaar, A., Martin, R. V., and Park, R. J.: Estimating ground-level PM_{2.5} using aerosol
524 optical depth determined from satellite remote sensing, *Journal of Geophysical Research*
525 *Atmospheres*, 111, 1–10, <https://doi.org/10.1029/2005JD006996>, 2006.

526 van Donkelaar, A., Martin, R. V., Brauer, M., Kahn, R., Levy, R., Verduzco, C., and Villeneuve,
527 P. J.: Global estimates of ambient fine particulate matter concentrations from satellite-based
528 aerosol optical depth: Development and application, *Environmental Health Perspectives*, 118,
529 847–855, <https://doi.org/10.1289/ehp.0901623>, 2010.

530 van Donkelaar, A., Martin, R. V., Spurr, R. J. D., Drury, E., Remer, L. A., Levy, R. C., and Wang,
531 J.: Optimal estimation for global ground-level fine particulate matter concentrations, *Journal of*
532 *Geophysical Research Atmospheres*, 118, 5621–5636, <https://doi.org/10.1002/jgrd.50479>, 2013.

533 van Donkelaar, A., Martin, R. V., Spurr, R. J. D., and Burnett, R. T.: High-Resolution Satellite-
534 Derived PM_{2.5} from Optimal Estimation and Geographically Weighted Regression over North
535 America, *Environmental Science and Technology*, 49, 10482–10491,
536 <https://doi.org/10.1021/acs.est.5b02076>, 2015.

537 van Donkelaar, A., Martin, R. V., Brauer, M., Hsu, N. C., Kahn, R. A., Levy, R. C., Lyapustin, A.,
538 Sayer, A. M., and Winker, D. M.: Global Estimates of Fine Particulate Matter using a Combined
539 Geophysical-Statistical Method with Information from Satellites, Models, and Monitors,
540 *Environmental Science and Technology*, 50, 3762–3772, <https://doi.org/10.1021/acs.est.5b05833>,
541 2016.

542 Eastham, S. D., Long, M. S., Keller, C. A., Lundgren, E., Yantosca, R. M., Zhuang, J., Li, C., Lee,
543 C. J., Yannetti, M., Auer, B. M., Clune, T. L., Kouatchou, J., Putman, W. M., Thompson, M. A.,
544 Trayanov, A. L., Molod, A. M., Martin, R. V., and Jacob, D. J.: GEOS-Chem high performance
545 (GCHP v11-02c): A next-generation implementation of the GEOS-Chem chemical transport
546 model for massively parallel applications, *Geoscientific Model Development*, 11, 2941–2953,
547 <https://doi.org/10.5194/gmd-11-2941-2018>, 2018.

548 Fairlie, D. T., Jacob, D. J., and Park, R. J.: The impact of transpacific transport of mineral dust in
549 the United States, *Atmospheric Environment*, 41, 1251–1266,
550 <https://doi.org/10.1016/j.atmosenv.2006.09.048>, 2007.

551 Ford, B. and Heald, C. L.: Exploring the uncertainty associated with satellite-based estimates of
552 premature mortality due to exposure to fine particulate matter, *Atmospheric Chemistry and Physics*
553 *Discussions*, 15, 25329–25380, <https://doi.org/10.5194/acpd-15-25329-2015>, 2015.

554 Fountoukis, C. and Nenes, A.: ISORROPIAII: A computationally efficient thermodynamic
555 equilibrium model for K⁺-Ca²⁺-Mg²⁺-NH₄⁺-Na⁺-SO₄²⁻-NO₃⁻-Cl⁻-H₂O aerosols, *Atmospheric*
556 *Chemistry and Physics*, 7, 4639–4659, <https://doi.org/10.5194/acp-7-4639-2007>, 2007.

557 Geng, G., Zhang, Q., Tong, D., Li, M., Zheng, Y., Wang, S., and He, K.: Chemical composition
558 of ambient PM_{2.5} over China and relationship to precursor emissions during 2005-2012,
559 *Atmospheric Chemistry and Physics*, 17, 9187–9203, <https://doi.org/10.5194/acp-17-9187-2017>,
560 2017.

561 Giles, D. M., Sinyuk, A., Sorokin, M. G., Schafer, J. S., Smirnov, A., Slutsker, I., Eck, T. F.,
562 Holben, B. N., Lewis, J. R., Campbell, J. R., Welton, E. J., Korokin, S. V., and Lyapustin, A. I.:
563 Advancements in the Aerosol Robotic Network (AERONET) Version 3 database - Automated
564 near-real-time quality control algorithm with improved cloud screening for Sun photometer
565 aerosol optical depth (AOD) measurements, *Atmospheric Measurement Techniques*, 12, 169–209,
566 <https://doi.org/10.5194/amt-12-169-2019>, 2019.

567 Guo, J., Xia, F., Zhang, Y., Liu, H., Li, J., Lou, M., He, J., Yan, Y., Wang, F., Min, M., and Zhai,
568 P.: Impact of diurnal variability and meteorological factors on the PM_{2.5} - AOD relationship:
569 Implications for PM_{2.5} remote sensing, *Environmental Pollution*, 221, 94–104,
570 <https://doi.org/10.1016/j.envpol.2016.11.043>, 2017.

571 Gupta, P., Christopher, S. A., Wang, J., Gehrig, R., Lee, Y., and Kumar, N.: Satellite remote
572 sensing of particulate matter and air quality assessment over global cities, *Atmospheric
573 Environment*, 40, 5880–5892, <https://doi.org/10.1016/j.atmosenv.2006.03.016>, 2006.

574 Hammer, M. S., Martin, R. V., Van Donkelaar, A., Buchard, V., Torres, O., Ridley, D. A., and
575 Spurr, R. J. D.: Interpreting the ultraviolet aerosol index observed with the OMI satellite
576 instrument to understand absorption by organic aerosols: Implications for atmospheric oxidation
577 and direct radiative effects, *Atmospheric Chemistry and Physics*, 16, 2507–2523,
578 <https://doi.org/10.5194/acp-16-2507-2016>, 2016.

579 Hao, H., Wang, Y., Zhu, Q., Zhang, H., Rosenberg, A., Schwartz, J., Amini, H., van Donkelaar,
580 A., Martin, R., Liu, P., Weber, R., Russel, A., Yitshak-sade, M., Chang, H., and Shi, L.: National
581 Cohort Study of Long-Term Exposure to PM_{2.5} Components and Mortality in Medicare American
582 Older Adults, *Environ. Sci. Technol.*, 57, 6835–6843, <https://doi.org/10.1021/acs.est.2c07064>,
583 2023.

584 He, Q., Wang, M., and Yim, S. H. L.: The spatiotemporal relationship between PM_{2.5} and aerosol
585 optical depth in China: Influencing factors and implications for satellite PM_{2.5} estimations using
586 MAIAC aerosol optical depth, *Atmospheric Chemistry and Physics*, 21, 18375–18391,
587 <https://doi.org/10.5194/acp-21-18375-2021>, 2021.

588 Heald, C. L., Collett, J. L., Lee, T., Benedict, K. B., Schwandner, F. M., Li, Y., Clarisse, L.,
589 Hurtmans, D. R., Van Damme, M., Clerbaux, C., Coheur, P. F., Philip, S., Martin, R. V., and Pye,
590 H. O. T.: Atmospheric ammonia and particulate inorganic nitrogen over the United States,
591 *Atmospheric Chemistry and Physics*, 12, 10295–10312, [https://doi.org/10.5194/acp-12-10295-
592 2012](https://doi.org/10.5194/acp-12-10295-
592 2012), 2012.

593 Hoesly, R. M., Smith, S. J., Feng, L., Klimont, Z., Janssens-Maenhout, G., Pitkanen, T., Seibert,
594 J. J., Vu, L., Andres, R. J., Bolt, R. M., Bond, T. C., Dawidowski, L., Kholod, N., Kurokawa, J. I.,
595 Li, M., Liu, L., Lu, Z., Moura, M. C. P., O'Rourke, P. R., and Zhang, Q.: Historical (1750–2014)
596 anthropogenic emissions of reactive gases and aerosols from the Community Emissions Data
597 System (CEDS), *Geoscientific Model Development*, 11, 369–408, [https://doi.org/10.5194/gmd-
598 11-369-2018](https://doi.org/10.5194/gmd-
598 11-369-2018), 2018.

599 Hu, X., Waller, L. A., Lyapustin, A., Wang, Y., and Liu, Y.: 10-year spatial and temporal trends
600 of PM_{2.5} concentrations in the southeastern US estimated using high-resolution satellite data,
601 Atmospheric Chemistry and Physics, 14, 6301–6314, <https://doi.org/10.5194/acp-14-6301-2014>,
602 2014.

603 Jaeglé, L., Quinn, P. K., Bates, T. S., Alexander, B., and Lin, J. T.: Global distribution of sea salt
604 aerosols: New constraints from in situ and remote sensing observations, Atmospheric Chemistry
605 and Physics, 11, 3137–3157, <https://doi.org/10.5194/acp-11-3137-2011>, 2011.

606 Jin, Q., Crippa, P., and Pryor, S. C.: Spatial characteristics and temporal evolution of the
607 relationship between PM_{2.5} and aerosol optical depth over the eastern USA during 2003–2017,
608 Atmospheric Environment, 239, 117718, <https://doi.org/10.1016/j.atmosenv.2020.117718>, 2020.

609 Jin, X., Fiore, A. M., Curci, G., Lyapustin, A., Civerolo, K., Ku, M., Van Donkelaar, A., and
610 Martin, R. V.: Assessing uncertainties of a geophysical approach to estimate surface fine
611 particulate matter distributions from satellite-observed aerosol optical depth, Atmospheric
612 Chemistry and Physics, 19, 295–313, <https://doi.org/10.5194/acp-19-295-2019>, 2019.

613 Kim, P. S., Jacob, D. J., Fisher, J. A., Travis, K., Yu, K., Zhu, L., Yantosca, R. M., Sulprizio, M.
614 P., Jimenez, J. L., Campuzano-Jost, P., Froyd, K. D., Liao, J., Hair, J. W., Fenn, M. A., Butler, C.
615 F., Wagner, N. L., Gordon, T. D., Welti, A., Wennberg, P. O., Crounse, J. D., St. Clair, J. M., Teng,
616 A. P., Millet, D. B., Schwarz, J. P., Markovic, M. Z., and Perring, A. E.: Sources, seasonality, and
617 trends of southeast US aerosol: An integrated analysis of surface, aircraft, and satellite
618 observations with the GEOS-Chem chemical transport model, Atmospheric Chemistry and
619 Physics, 15, 10411–10433, <https://doi.org/10.5194/acp-15-10411-2015>, 2015.

620 Kondragunta, S., Veihelmann, B., and Chatfield, R. J.: Monitoring Surface PM_{2.5}: An
621 International Constellation Approach to Enhancing the Role of Satellite Observations,
622 <https://doi.org/10.25923/7SNZ-VN34>, 2022.

623 Kopke, P., Hess, M., Schult, I., and Shettle, E. P.: Global Aerosol Data Set, Max-Planck-Institut
624 Fur Meteorologie, Hamburg, [https://doi.org/Report No. 243](https://doi.org/Report%20No.%20243), 1997.

625 Latimer, R. N. C. and Martin, R. V.: Interpretation of measured aerosol mass scattering efficiency
626 over North America using a chemical transport model, Atmospheric Chemistry and Physics, 19,
627 2635–2653, <https://doi.org/10.5194/acp-19-2635-2019>, 2019.

628 Li, J., Carlson, B. E., and Lacis, A. A.: How well do satellite AOD observations represent the
629 spatial and temporal variability of PM_{2.5} concentration for the United States?, Atmospheric
630 Environment, 102, 260–273, <https://doi.org/10.1016/j.atmosenv.2014.12.010>, 2015.

631 Li, Y., Martin, R. V., Li, C., Boys, B. L., van Donkelaar, A., Meng, J., and Pierce, J. R.:
632 Development and evaluation of processes affecting simulation of diel fine particulate matter
633 variation in the GEOS-Chem model, Atmospheric Chemistry and Physics, 23, 12525–12543,
634 <https://doi.org/10.5194/ACP-23-12525-2023>, 2023.

635 Lin, H., Jacob, D. J., Lundgren, E. W., Sulprizio, M. P., Keller, C. A., Fritz, T. M., Eastham, S. D.,
636 Emmons, L. K., Campbell, P. C., Baker, B., Saylor, R. D., and Montuoro, R.: Harmonized
637 Emissions Component (HEMCO) 3.0 as a versatile emissions component for atmospheric models:
638 application in the GEOS-Chem, NASA GEOS, WRF-GC, CESM2, NOAA GEFS-Aerosol, and
639 NOAA UFS models, *Geoscientific Model Development*, 14, 5487–5506,
640 <https://doi.org/10.5194/gmd-14-5487-2021>, 2021.

641 Liu, H., Jacob, D. J., Bey, I., and Yantosca, R. M.: Constraints from ²¹⁰Pb and ⁷Be on wet
642 deposition and transport in a global three-dimensional chemical tracer model driven by assimilated
643 meteorological fields, *Journal of Geophysical Research Atmospheres*, 106, 12109–12128,
644 <https://doi.org/10.1029/2000JD900839>, 2001.

645 Liu, X., Turner, J. R., Hand, J. L., Schichtel, B. A., and Martin, R. V.: A Global-Scale Mineral
646 Dust Equation, *Journal of Geophysical Research: Atmospheres*, 127, e2022JD036937,
647 <https://doi.org/10.1029/2022JD036937>, 2022.

648 Liu, X., Turner, J. R., Oxford, C. R., McNeill, J., Walsh, B., Le Roy, E., Weagle, C. L., Stone, E.,
649 Zhu, H., Liu, W., Wei, Z., Hyslop, N. P., Giacomo, J., Dillner, A. M., Salam, A., Hossen, A., Islam,
650 Z., Abboud, I., Akoshile, C., Amador-Muñoz, O., Anh, N. X., Asfaw, A., Balasubramanian, R.,
651 Chang, R. Y.-W., Coburn, C., Dey, S., Diner, D. J., Dong, J., Farrah, T., Gahungu, P., Garland, R.
652 M., Grutter de la Mora, M., Hasheminassab, S., John, J., Kim, J., Kim, J. S., Langerman, K., Lee,
653 P.-C., Lestari, P., Liu, Y., Mamo, T., Martins, M., Mayol-Bracero, O. L., Naidoo, M., Park, S. S.,
654 Schechner, Y., Schofield, R., Tripathi, S. N., Windwer, E., Wu, M.-T., Zhang, Q., Brauer, M.,
655 Rudich, Y., and Martin, R. V.: Elemental Characterization of Ambient Particulate Matter for a
656 Globally Distributed Monitoring Network: Methodology and Implications, *ACS EST Air*,
657 <https://doi.org/10.1021/acsestair.3c00069>, 2024.

658 Lyapustin, A., Wang, Y., Korkin, S., and Huang, D.: MODIS Collection 6 MAIAC algorithm,
659 *Atmospheric Measurement Techniques*, 11, 5741–5765, [https://doi.org/10.5194/amt-11-5741-](https://doi.org/10.5194/amt-11-5741-2018)
660 2018, 2018.

661 Martin, R. V., Jacob, D. J., Yantosca, R. M., Chin, M., and Ginoux, P.: Global and regional
662 decreases in tropospheric oxidants from photochemical effects of aerosols, *Journal of Geophysical*
663 *Research: Atmospheres*, 108, <https://doi.org/10.1029/2002jd002622>, 2003.

664 Martin, R. V., Brauer, M., van Donkelaar, A., Shaddick, G., Narain, U., and Dey, S.: No one knows
665 which city has the highest concentration of fine particulate matter, *Atmospheric Environment: X*,
666 3, <https://doi.org/10.1016/j.aeaoa.2019.100040>, 2019.

667 Martin, R. V., Eastham, S. D., Bindle, L., Lundgren, E. W., Clune, T. L., Keller, C. A., Downs,
668 W., Zhang, D., Lucchesi, R. A., Sulprizio, M. P., Yantosca, R. M., Li, Y., Estrada, L., Putman, W.
669 M., Auer, B. M., Trayanov, L., Pawson, S., and Jacob, D. J.: Improved Advection , Resolution ,
670 Performance , and Community Access in the New Generation (Version 13) of the High
671 Performance GEOS-Chem Global Atmospheric Chemistry Model (GCHP), *Geoscientific Model*
672 *Development Discussions*, 720, 1–30, <https://doi.org/10.5194/gmd-2022-42>, 2022.

673 McDuffie, E. E., Martin, R. V., Spadaro, J. V., Burnett, R., Smith, S. J., O'Rourke, P., Hammer,
674 M. S., van Donkelaar, A., Bindle, L., Shah, V., Jaeglé, L., Luo, G., Yu, F., Adeniran, J. A., Lin, J.,
675 and Brauer, M.: Source sector and fuel contributions to ambient PM_{2.5} and attributable mortality
676 across multiple spatial scales, *Nature Communications*, 12, 1–12, [https://doi.org/10.1038/s41467-](https://doi.org/10.1038/s41467-021-23853-y)
677 021-23853-y, 2021.

678 Meng, J., Martin, R. V., Ginoux, P., Hammer, M., Sulprizio, M. P., Ridley, D. A., and Van
679 Donkelaar, A.: Grid-independent high-resolution dust emissions (v1.0) for chemical transport
680 models: Application to GEOS-Chem (12.5.0), *Geoscientific Model Development*, 14, 4249–4260,
681 <https://doi.org/10.5194/gmd-14-4249-2021>, 2021.

682 Miao, R., Chen, Q., Zheng, Y., Cheng, X., Sun, Y., Palmer, P. I., Shrivastava, M., Guo, J., Zhang,
683 Q., Liu, Y., Tan, Z., Ma, X., Chen, S., Zeng, L., Lu, K., and Zhang, Y.: Model bias in simulating
684 major chemical components of PM_{2.5} in China, *Atmospheric Chemistry and Physics*, 20, 12265–
685 12284, <https://doi.org/10.5194/acp-20-12265-2020>, 2020.

686 Nguyen, T. T. N., Pham, H. V., Lasko, K., Bui, M. T., Laffly, D., Jourdan, A., and Bui, H. Q.:
687 Spatiotemporal analysis of ground and satellite-based aerosol for air quality assessment in the
688 Southeast Asia region, *Environmental Pollution*, 255, 113106,
689 <https://doi.org/10.1016/j.envpol.2019.113106>, 2019.

690 CEDS: <https://www.pnnl.gov/projects/ceds>, last access: 6 July 2024.

691 Pai, S. J., Heald, C. L., Pierce, J. R., Farina, S. C., Marais, E. A., Jimenez, J. L., Campuzano-Jost,
692 P., Nault, B. A., Middlebrook, A. M., Coe, H., Shilling, J. E., Bahreini, R., Dingle, J. H., and Vu,
693 K.: An evaluation of global organic aerosol schemes using airborne observations, *Atmospheric*
694 *Chemistry and Physics*, 20, 2637–2665, <https://doi.org/10.5194/acp-20-2637-2020>, 2020.

695 Park, R. J., Jacob, D. J., Chin, M., and Martin, R. V.: Sources of carbonaceous aerosols over the
696 United States and implications for natural visibility, *Journal of Geophysical Research*
697 *Atmospheres*, 108, <https://doi.org/10.1029/2002jd003190>, 2003.

698 Philip, S., Martin, R. V., van Donkelaar, A., Lo, J. W.-H., Wang, Y., Chen, D., Zhang, L.,
699 Kasibhatla, P. S., Wang, S., Zhang, Q., Lu, Z., Streets, D. G., Bittman, S., and Macdonald, D. J.:
700 Global Chemical Composition of Ambient Fine Particulate Matter for Exposure Assessment,
701 *Environ. Sci. Technol.*, 48, 13060–13068, <https://doi.org/10.1021/es502965b>, 2014a.

702 Philip, S., Martin, R. V., Pierce, J. R., Jimenez, J. L., Zhang, Q., Canagaratna, M. R., Spracklen,
703 D. V., Nowlan, C. R., Lamsal, L. N., Cooper, M. J., and Krotkov, N. A.: Spatially and seasonally
704 resolved estimate of the ratio of organic mass to organic carbon, *Atmospheric Environment*, 87,
705 34–40, <https://doi.org/10.1016/j.atmosenv.2013.11.065>, 2014b.

706 Philip, S., Martin, R. V., Snider, G., Weagle, C. L., Van Donkelaar, A., Brauer, M., Henze, D. K.,
707 Klimont, Z., Venkataraman, C., Guttikunda, S. K., and Zhang, Q.: Anthropogenic fugitive,
708 combustion and industrial dust is a significant, underrepresented fine particulate matter source in
709 global atmospheric models, *Environmental Research Letters*, 12, [https://doi.org/10.1088/1748-](https://doi.org/10.1088/1748-9326/aa65a4)
710 9326/aa65a4, 2017.

- 711 Pinault, L., Tjepkema, M., Crouse, D. L., Weichenthal, S., van Donkelaar, A., Martin, R. V.,
712 Brauer, M., Chen, H., and Burnett, R. T.: Risk estimates of mortality attributed to low
713 concentrations of ambient fine particulate matter in the Canadian community health survey cohort,
714 *Environmental Health*, 15, 18, <https://doi.org/10.1186/s12940-016-0111-6>, 2016.
- 715 Prank, M., Sofiev, M., Tsyro, S., Hendriks, C., Semeena, V., Vazhappilly Francis, X., Butler, T.,
716 Denier van der Gon, H., Friedrich, R., Hendricks, J., Kong, X., Lawrence, M., Righi, M., Samaras,
717 Z., Sausen, R., Kukkonen, J., and Sokhi, R.: Evaluation of the performance of four chemical
718 transport models in predicting the aerosol chemical composition in Europe in 2005, *Atmospheric*
719 *Chemistry and Physics*, 16, 6041–6070, <https://doi.org/10.5194/acp-16-6041-2016>, 2016.
- 720 Sayer, A. M., Munchak, L. A., Hsu, N. C., Levy, R. C., Bettenhausen, C., and Jeong, M. J.: MODIS
721 Collection 6 aerosol products: Comparison between Aqua’s e-Deep Blue, Dark Target, and
722 “merged” data sets, and usage recommendations, *Journal of Geophysical Research: Atmospheres*,
723 119, 13,965–13,989, <https://doi.org/10.1002/2014JD022453>, 2014.
- 724 Schubert, S. D., Rood, R. B., and Pfaendtner, J.: An Assimilated Dataset for Earth Science
725 Applications, *Bulletin of the American Meteorological Society*, 74, 2331–2342,
726 [https://doi.org/10.1175/1520-0477\(1993\)074<2331:AADFES>2.0.CO;2](https://doi.org/10.1175/1520-0477(1993)074<2331:AADFES>2.0.CO;2), 1993.
- 727 Sha, T., Ma, X., Jia, H., Tian, R., Chang, Y., Cao, F., and Zhang, Y.: Aerosol chemical component:
728 Simulations with WRF-Chem and comparison with observations in Nanjing, *Atmospheric*
729 *Environment*, 218, 116982, <https://doi.org/10.1016/j.atmosenv.2019.116982>, 2019.
- 730 Shimadera, H., Hayami, H., Chatani, S., Morino, Y., Mori, Y., Morikawa, T., Yamaji, K., and
731 Ohara, T.: Sensitivity analyses of factors influencing CMAQ performance for fine particulate
732 nitrate, *Journal of the Air & Waste Management Association*, 64, 374–387,
733 <https://doi.org/10.1080/10962247.2013.778919>, 2014.
- 734 Snider, G., Weagle, C. L., Murdymootoo, K. K., Ring, A., Ritchie, Y., Stone, E., Walsh, A.,
735 Akoshile, C., Anh, N. X., Balasubramanian, R., Brook, J., Qonitan, F. D., Dong, J., Griffith, D.,
736 He, K., Holben, B. N., Kahn, R., Lagrosas, N., Lestari, P., Ma, Z., Misra, A., Norford, L. K., Quel,
737 E. J., Salam, A., Schichtel, B., Segev, L., Tripathi, S., Wang, C., Yu, C., Zhang, Q., Zhang, Y.,
738 Brauer, M., Cohen, A., Gibson, M. D., Liu, Y., Martins, J. V., Rudich, Y., and Martin, R. V.:
739 Variation in global chemical composition of PM_{2.5}: emerging results from SPARTAN,
740 *Atmospheric Chemistry and Physics*, 16, 9629–9653, <https://doi.org/10.5194/acp-16-9629-2016>,
741 2016.
- 742 Travis, K. R., Crawford, J. H., Chen, G., Jordan, C. E., Nault, B. A., Kim, H., Jimenez, J. L.,
743 Campuzano-Jost, P., Dibb, J. E., Woo, J. H., Kim, Y., Zhai, S., Wang, X., McDuffie, E. E., Luo,
744 G., Yu, F., Kim, S., Simpson, I. J., Blake, D. R., Chang, L., and Kim, M. J.: Limitations in
745 representation of physical processes prevent successful simulation of PM_{2.5} during KORUS-AQ,
746 *Atmospheric Chemistry and Physics*, 22, 7933–7958, <https://doi.org/10.5194/acp-22-7933-2022>,
747 2022.
- 748 Wang, Q., Jacob, D. J., Spackman, J. R., Perring, A. E., Schwarz, J. P., Moteki, N., Marais, E. A.,
749 Ge, C., Wang, J., and Barrett, S. R. H.: Global budget and radiative forcing of black carbon aerosol:

750 Constraints from pole-to-pole (HIPPO) observations across the Pacific, *Journal of Geophysical*
751 *Research*, 119, 195–206, <https://doi.org/10.1002/2013JD020824>, 2014.

752 Wang, Y., Jacob, D. J., and Logan, J. A.: Global simulation of tropospheric O₃-NO_x-hydrocarbon
753 chemistry - 1. Model formulation, *Journal of Geophysical Research: Atmospheres*, 103, 10713–
754 10725, <https://doi.org/10.1029/98jd00158>, 1998.

755 Weagle, C. L., Snider, G., Li, C., Van Donkelaar, A., Philip, S., Bissonnette, P., Burke, J., Jackson,
756 J., Latimer, R., Stone, E., Abboud, I., Akoshile, C., Anh, N. X., Brook, J. R., Cohen, A., Dong, J.,
757 Gibson, M. D., Griffith, D., He, K. B., Holben, B. N., Kahn, R., Keller, C. A., Kim, J. S., Lagrosas,
758 N., Lestari, P., Khian, Y. L., Liu, Y., Marais, E. A., Martins, J. V., Misra, A., Muliane, U., Pratiwi,
759 R., Quel, E. J., Salam, A., Segev, L., Tripathi, S. N., Wang, C., Zhang, Q., Brauer, M., Rudich, Y.,
760 and Martin, R. V.: Global Sources of Fine Particulate Matter: Interpretation of PM_{2.5} Chemical
761 Composition Observed by SPARTAN using a Global Chemical Transport Model, *Environmental*
762 *Science and Technology*, 52, 11670–11681, <https://doi.org/10.1021/acs.est.8b01658>, 2018.

763 Weichenthal, S., Pinault, L., Christidis, T., Burnett, R. T., Brook, J. R., Chu, Y., Crouse, D. L.,
764 Erickson, A. C., Hystad, P., Li, C., Martin, R. V., Meng, J., Pappin, A. J., Tjepkema, M., van
765 Donkelaar, A., Weagle, C. L., and Brauer, M.: How low can you go? Air pollution affects mortality
766 at very low levels, *Science Advances*, 8, eabo3381, <https://doi.org/10.1126/sciadv.abo3381>, 2022.

767 Wendt, E. A., Ford, B., Cheeseman, M., Rosen, Z., Pierce, J. R., H. Jathar, S., L'Orange, C., Quinn,
768 C., Long, M., Mehaffy, J., D. Miller-Lionberg, D., H. Hagan, D., and Volckens, J.: A national
769 crowdsourced network of low-cost fine particulate matter and aerosol optical depth monitors:
770 results from the 2021 wildfire season in the United States, *Environmental Science: Atmospheres*,
771 3, 1563–1575, <https://doi.org/10.1039/D3EA00086A>, 2023.

772 Weng, H., Lin, J., Martin, R., Millet, D. B., Jaeglé, L., Ridley, D., Keller, C., Li, C., Du, M., and
773 Meng, J.: Global high-resolution emissions of soil NO_x, sea salt aerosols, and biogenic volatile
774 organic compounds, *Scientific Data*, 7, 1–15, <https://doi.org/10.1038/s41597-020-0488-5>, 2020.

775 van der Werf, G. R., Randerson, J. T., Giglio, L., Van Leeuwen, T. T., Chen, Y., Rogers, B. M.,
776 Mu, M., Van Marle, M. J. E., Morton, D. C., Collatz, G. J., Yokelson, R. J., and Kasibhatla, P. S.:
777 Global fire emissions estimates during 1997-2016, *Earth System Science Data*, 9, 697–720,
778 <https://doi.org/10.5194/essd-9-697-2017>, 2017.

779 White, W. H., Trzepla, K., Hyslop, N. P., and Schichtel, B. A.: A critical review of filter
780 transmittance measurements for aerosol light absorption, and de novo calibration for a decade of
781 monitoring on PTFE membranes, *Aerosol Science and Technology*, 50, 984–1002,
782 <https://doi.org/10.1080/02786826.2016.1211615>, 2016.

783 Xin, J., Zhang, Q., Wang, L., Gong, C., Wang, Y., Liu, Z., and Gao, W.: The empirical relationship
784 between the PM_{2.5} concentration and aerosol optical depth over the background of North China
785 from 2009 to 2011, *Atmospheric Research*, 138, 179–188,
786 <https://doi.org/10.1016/j.atmosres.2013.11.001>, 2014.

787 Yang, Q., Yuan, Q., Yue, L., Li, T., Shen, H., and Zhang, L.: The relationships between PM_{2.5}
788 and aerosol optical depth (AOD) in mainland China: About and behind the spatio-temporal
789 variations, *Environmental Pollution*, 248, 526–535, <https://doi.org/10.1016/j.envpol.2019.02.071>,
790 2019.

791 Zhai, S., Jacob, D., Brewer, J., Li, K., Moch, J., Kim, J., Lee, S., Lim, H., Lee, H. C., Kuk, S. K.,
792 Park, R., Jeong, J., Wang, X., Liu, P., Luo, G., Yu, F., Meng, J., Martin, R., Travis, K., Hair, J.,
793 Anderson, B., Dibb, J., Jimenez, J., Campuzano-Jost, P., Nault, B., Woo, J.-H., Kim, Y., Zhang,
794 Q., and Liao, H.: Interpretation of geostationary satellite aerosol optical depth (AOD) over East
795 Asia in relation to fine particulate matter (PM_{2.5}): insights from the KORUS-AQ aircraft
796 campaign and seasonality, *Atmospheric Chemistry and Physics*, 1–23,
797 <https://doi.org/10.5194/acp-2021-413>, 2021.

798 Zhang, H., Hoff, R. M., and Engel-Cox, J. A.: The relation between moderate resolution imaging
799 spectroradiometer (MODIS) aerosol optical depth and PM_{2.5} over the United States: A
800 geographical comparison by U.S. Environmental Protection Agency regions, *Journal of the Air
801 and Waste Management Association*, 59, 1358–1369, [https://doi.org/10.3155/1047-
802 3289.59.11.1358](https://doi.org/10.3155/1047-3289.59.11.1358), 2009.

803 Zhang, L., Jacob, D. J., Knipping, E. M., Kumar, N., Munger, J. W., Carouge, C. C., Van
804 Donkelaar, A., Wang, Y. X., and Chen, D.: Nitrogen deposition to the United States: Distribution,
805 sources, and processes, *Atmospheric Chemistry and Physics*, 12, 4539–4554,
806 <https://doi.org/10.5194/ACP-12-4539-2012>, 2012.

807 Zhang, L., Kok, J. F., Henze, D. K., Li, Q., and Zhao, C.: Improving simulations of fine dust
808 surface concentrations over the western United States by optimizing the particle size distribution,
809 *Geophysical Research Letters*, 40, 3270–3275, <https://doi.org/10.1002/grl.50591>, 2013.

810 Zhao, B., Jiang, J. H., Diner, D. J., Su, H., Gu, Y., Liou, K.-N., Jiang, Z., Huang, L., Takano, Y.,
811 Fan, X., and Omar, A. H.: Intra-annual variations of regional aerosol optical depth, vertical
812 distribution, and particle types from multiple satellite and ground-based observational datasets,
813 *Atmospheric Chemistry and Physics*, 18, 11247–11260, [https://doi.org/10.5194/acp-18-11247-
814 2018](https://doi.org/10.5194/acp-18-11247-2018), 2018.

815 Zhu, H., Martin, R. V., Croft, B., Zhai, S., Li, C., Bindle, L., Pierce, J. R., Chang, R. Y. W.,
816 Anderson, B. E., Ziemba, L. D., Hair, J. W., Ferrare, R. A., Hostetler, C. A., Singh, I., Chatterjee,
817 D., Jimenez, J. L., Campuzano-Jost, P., Nault, B. A., Dibb, J. E., Schwarz, J. S., and Weinheimer,
818 A.: Parameterization of size of organic and secondary inorganic aerosol for efficient representation
819 of global aerosol optical properties, *Atmospheric Chemistry and Physics*, 23, 5023–5042,
820 <https://doi.org/10.5194/ACP-23-5023-2023>, 2023.

821

822